Protein kinase A drives paracrine crisis and WNT4-dependent testis tumor in Carney complex

Cyril Djari, … , Antoine Martinez, Anne-Marie Lefrançois-Martinez
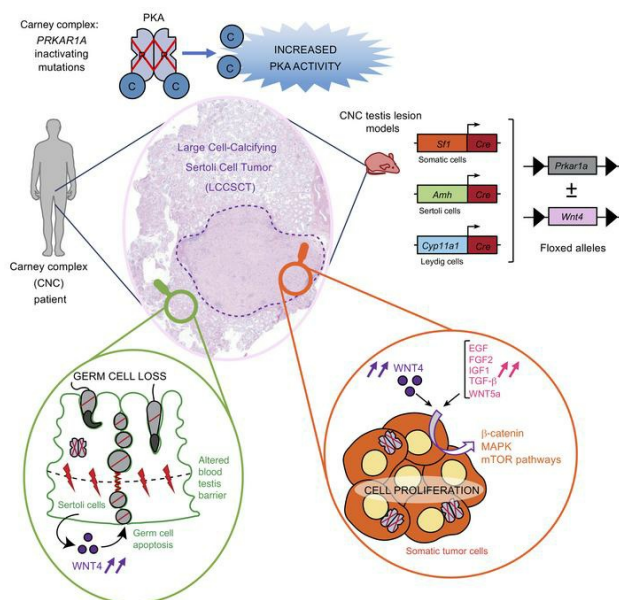
Research Article   Endocrinology   Reproductive biology

Graphical abstract

Protein kinase A drives paracrine crisis and WNT4-dependent testis tumor in Carney complex

Cyril Djari,[1] Isabelle Sahut-Barnola,[1] Amandine Septier,[1] Ingrid Plotton,[2] Nathanaëlle Montanier,[1,3] Damien Dufour,[1] Adrien Levasseur,[1] James Wilmouth Jr.,[1] Jean-Christophe Pointud,[1] Fabio R. Faucz,[4] Crystal Kamilaris,[4] Antoine-Guy Lopez,[5] Florian Guillou,[6] Amanda Swain,[7] Seppo J. Vainio,[8] Igor Tauveron,[1,3] Pierre Val,[1] Hervé Lefebvre,[5] Constantine A. Stratakis,[4] Antoine Martinez,[1] and Anne-Marie Lefrançois-Martinez[1]

[1]iGReD, Université Clermont-Auvergne, CNRS6293, INSERM U1103, Clermont-Ferrand, France. [2]UM Pathologies Endocriniennes Rénales Musculaires et Mucoviscidose, Hospices Civils de Lyon, Bron, France. [3]Université Clermont-Auvergne, CHU Clermont-Ferrand, Clermont-Ferrand, France. [4]Section on Endocrinology and Genetics, Eunice Kennedy Shriver National Institute of Child Health and Human Development (NICHD), NIH, Bethesda, Maryland, USA. [5]Normandie University, UNIROUEN, INSERM U1239, Rouen University Hospital, Department of Endocrinology, Diabetology and Metabolic Diseases and CIC-CRB 140h4, Rouen, France. [6] PRC, INRAE, CNRS, IFCE, Tours University, Nouzilly, France. [7]Division of Cancer Biology, Institute of Cancer Research, London, United Kingdom. [8]Laboratory of Developmental Biology, Faculty of Biochemistry and Molecular Medicine, Biocenter Oulu, University of Oulu, Oulu, Finland.

Large-cell calcifying Sertoli cell tumors (LCCSCTs) are among the most frequent lesions occurring in male Carney complex (CNC) patients. Although they constitute a key diagnostic criterion for this rare multiple neoplasia syndrome resulting from inactivating mutations of the tumor suppressor *PRKAR1A*, leading to unrepressed PKA activity, LCCSCT pathogenesis and origin remain elusive. Mouse models targeting *Prkar1a* inactivation in all somatic populations or separately in each cell type were generated to decipher the molecular and paracrine networks involved in the induction of CNC testis lesions. We demonstrate that the *Prkar1a* mutation was required in both stromal and Sertoli cells for the occurrence of LCCSCTs. Integrative analyses comparing transcriptomic, immunohistological data and phenotype of mutant mouse combinations led to the understanding of human LCCSCT pathogenesis and demonstrated PKA-induced paracrine molecular circuits in which the aberrant WNT4 signal production is a limiting step in shaping intratubular lesions and tumor expansion both in a mouse model and in human CNC testes.

Introduction

Carney complex (CNC) is a rare multiple neoplasia syndrome mainly associated with inactivating mutations of the *PRKAR1A* gene encoding the R1α subunit of the PKA, which results in overactive PKA signaling (1). It is characterized by pigmented lesions of the skin and mucosae, cardiac, cutaneous, and other myxomatous tumors, and multiple other endocrine and nonendocrine neoplasms (2, 3). Approximatively 70% of patients are estimated to develop large-cell calcifying Sertoli cell tumors (LCCSCTs) (2, 4). LCCSCT is a testicular sex cord stromal tumor (SCST) subtype characterized by bilateral and multifocal masses caused by inactivating mutations of *PRKAR1A* (17q22–24) associated with CNC, but is also described in Peutz-Jeghers syndrome (PJS) caused by inactivating mutations of *STK11* (19p13.3) (5, 6). LCCSCTs developing in the case of CNC (CNC-LCCSCTs) are mostly benign tumors with low malignant potential, may be diagnosed from childhood by sonographic examination, and are associated with precocious puberty in some cases (7, 8). In engineered *Prkar1a+/−* mice, loss of heterozygosity for the *Prkar1a* locus has been implicated in the tumorigenesis process for CNC-related neoplasia (9), indicating

that the resulting constitutive PKA activity plays an oncogenic role in specific tissues (10). The current management for LCCSCTs consists of the resection of the primary tumor due to the limited effect of chemotherapy and radiation treatments. However, the tumor discriminant markers are insufficient to allow early detection of a potential recurrence and to distinguish LCCSCTs from other SCSTs. Histological analyses highlight various tissue alterations (11). Moderate tubular damages characterized by spermatogenesis defects, calcifications, peritubular fibrosis, and composite tumor mass combined with Sertoli cell (SC) proliferating nodules have been described (12, 13). LCCSCT presence is systematically associated with increased production of inhibin-α, S100, calretinin, and β-catenin, but its molecular status is still incompletely determined due to low LCCSCT incidence (11, 14, 15). Therefore the molecular mechanisms and the cellular events involved in LCCSCT pathogenesis remain to be understood to improve their management. Moreover, the reproductive alterations have been poorly investigated in male CNC patients, especially concerning their fertility as well as their testis endocrine activity.

In embryo, SCs and Leydig cells (LCs) arise from a common pool of SF1+ (also called NR5A1) progenitor cells under the control of coordinate genetic and paracrine mechanisms triggered by the male-determining SRY- and SOX9-induced programs to counteract the female RSPO1/WNT4/β-catenin and FOXL2 pathways (16). At adulthood, testicular physiology carries out exocrine and endocrine functions: SCs support germ cell (GC) nursing, includ-

ing growth and differentiation in seminiferous tubules (STs), and LCs produce androgens in the interstitial compartment. Pituitary follicle-stimulating hormone (FSH) and luteinizing hormone (LH) are the main regulators of the adult SC and LC functions through their respective specific G protein–coupled receptors, FSH-R and LH-R, both interacting with a number of intracellular effectors, among which the cAMP/PKA pathway plays a central role. Activating mutations of human FSH-R and LH-R resulting in permanent PKA activity have been described for several years, and their physiological outcomes have been extensively studied through biochemical and functional approaches, including mutant mouse models (17–20). Whether activating mutations of the gonadotropin receptors are involved in tumor development is not yet clear, and their pathological outcomes do not overlap with the testis CNC lesions etiology. The objective of our work was to identify the molecular networks (deregulated by PKA activation) that cause the resulting cellular alterations found in the CNC testis. We generated several genetic mouse models lacking *Prkar1a*, either in all somatic testicular cells arising from fetal somatic progenitors (prKO model) or exclusively in SC (srKO model) or LC (lrKO model). The ontogenetic follow-up of the mutant mouse testes, together with genetic manipulation of the catalytic PKA subunit and WNT4 signal, should provide a readout of the sequence of histological, molecular, and endocrine modifications arising in human LCCSCTs from CNC patients.

Results

Prkar1a loss in mouse testicular somatic cells induces LCCSCT-like lesions. *Sf1:Cre,Prkar1a$^{fl/fl}$* mice (prKO mice) were generated to identify the underlying mechanisms of CNC-LCCSCT lesions by targeting early *Prkar1a* inactivation (E10.5) in somatic testis cells (Supplemental Figure 1, A and B; supplemental material available online with this article; https://doi.org/10.1172/JCI146910DS1). The use of the *Rosa26R-mtmg* reporter locus confirmed that the recombination affected all somatic testis cell types, excluding the GC population as previously described (ref. 21 and Supplemental Figure 1, A–C), and reverse-transcription quantitative PCR (RT-qPCR) analyses confirmed a robust reduction in *Prkar1a* mRNA levels in prKO testes (Supplemental Figure 1D). The mutant mouse colony setup revealed that prKO male mice were sterile beginning with the onset of puberty due to a lack of spermatozoa production and displayed a disrupted gonadotropic axis, with collapsed FSH and LH levels associated with hypertestosteronemia (Supplemental Figure 1, E–G). In contrast, 2-month-old *Sf1:cre,Prkar1a$^{fl/fl}$,Prkaca$^{-/+}$* male mice, harboring *Prkaca* haploinsufficiency with decreased PKA catalytic activity, retained healthy testis histology, indicating that testis failures in prKO mice were mostly due to PKA overactivation (Supplemental Figure 2, A–E). Masson's trichrome and H&E staining revealed that 2- and 4-month-old prKO mice exhibited a severe gonadic dysplasia with seminiferous compartment disorganization. Further analyses highlighted calcification areas using alizarin red S coloration, peritubular basal lamina thickening attested by laminin B1 immunostaining, and GC loss in close similarity with human CNC-LCCSCT histology (Figure 1, A and B, Supplemental Figure 1, H–J, and Supplemental Figure 3). Transcript levels for the SCST current molecular markers, i.e., *Calb2*, *Ctnnb1*, *Inha*, and *S100a1*, were strongly

increased in the 4-month-old prKO testes compared with that of WT (Figure 1C). Moreover, hypertrophic blood vessels and early bilateral proliferative stromal tumor mass expansion, attested by the increased stromal proliferating cell nuclear antigen (PCNA) index, were observed in 4-month-old mutant testes, whereas only limited stromal hyperplastic areas arose without tubular defect in 2-week-old mutant testes (Figure 1, A, D, and E, and Supplemental Figure 1K). In contrast, heterozygous *Sf1:Cre,Prkar1a$^{fl/+}$* littermates displayed a healthy testicular phenotype, similarly to that of the *Prkar1a$^{fl/fl}$* mice. All these observations demonstrated that loss of *Prkar1a* in mice phenocopied all tissue defects found in testes from CNC patients. To gain insight into the gene expression profiles associated with the prKO testis lesion setup, we conducted comparative microarray analyses on gene expression in 2-week-old and 2-month-old prKO and WT testes. Transcriptomic analyses revealed 1328 significantly deregulated genes in adult prKO mice (676 up- and 652 downregulated genes), whereas only 93 genes were deregulated at 2 weeks in mutant testes: 90 up- and 3 downregulated genes compared with WT (abs[log$_2$ fold change (FC)] > 1, adj. *P* < 0.05; Figure 1, F and G, and Supplemental Data File 2). These data emphasized the delayed functional response to *Prkar1a* inactivation that was triggered from the early fetal gonadal stage (Supplemental Figure 1B). Gene Ontology (GO) analyses performed on transcriptomic data from 2-week-old testes highlighted an increased expression in genes involved in steroid metabolism, whereas gene signatures associated with intratubular cell homeostasis were virtually unaffected (Supplemental Data Files 1–3). Consistent with these observations, hormonal assays revealed significant 134-fold increased testosterone levels in 17-day-old prKO testes (5.39 ng/organ) compared with WT (0.04 ng/organ) (plasma testosterone levels = 16.01 ng/mL ± 5.12 in prKO vs. 0.16 ng/mL ± 0.04 in WT), whereas testosterone levels were unchanged in the plasma of 5-day-old prKO mice (0.27 ng/mL ± 0.12) compared with WT (0.14 ng/mL ± 0.04). In 2-month-old prKO mice, unbiased GO and Kyoto Encyclopedia of Genes and Genomes (KEGG) analyses revealed a negative enrichment in signatures associated with spermatogenesis and sperm motility and a positive enrichment in gene expression involved in tissue reorganization and metabolic processes (Figure 1H), indicating that *Prkar1a* gene inactivation resulted in complex and deep disruption of adult testis function and somatic cell tumor formation.

ST defects are associated with Prkar1a loss in SCs. *Sf1:Cre*-mediated recombination in testis targeted both supporting and stromal cells and resulted in a complex phenotype in adult prKO mice with intratubular and stromal compartment alterations that could be amplified by reciprocal dysregulated paracrine signals. To unravel the impact of cell-specific *Prkar1a* loss in global LCCSCT pathogenesis, we generated lrKO (*Scc-Cre,Prkar1a$^{fl/fl}$*) and srKO (*Amh-Cre,Prkar1a$^{fl/fl}$*) mouse models with either LC- or SC-specific *Prkar1a* invalidation triggered from E13.5 and E15, respectively, using *Cyp11a1:Cre* or *Amh:Cre* drivers (22, 23). The cell specificity of recombination was confirmed by analyzing *Rosa26R-mtmg* reporter activity (Supplemental Figure 4, A–D). Similarly to WT, 2-month-old lrKO mice were fertile and showed healthy testicular histology (Figure 2, A–E) devoid of stromal hyperplasia or tumor expansion. However, like prKO mice, adult lrKO male mice developed hypertestosteronemia (Supplemental Figure 4G). Transcrip-
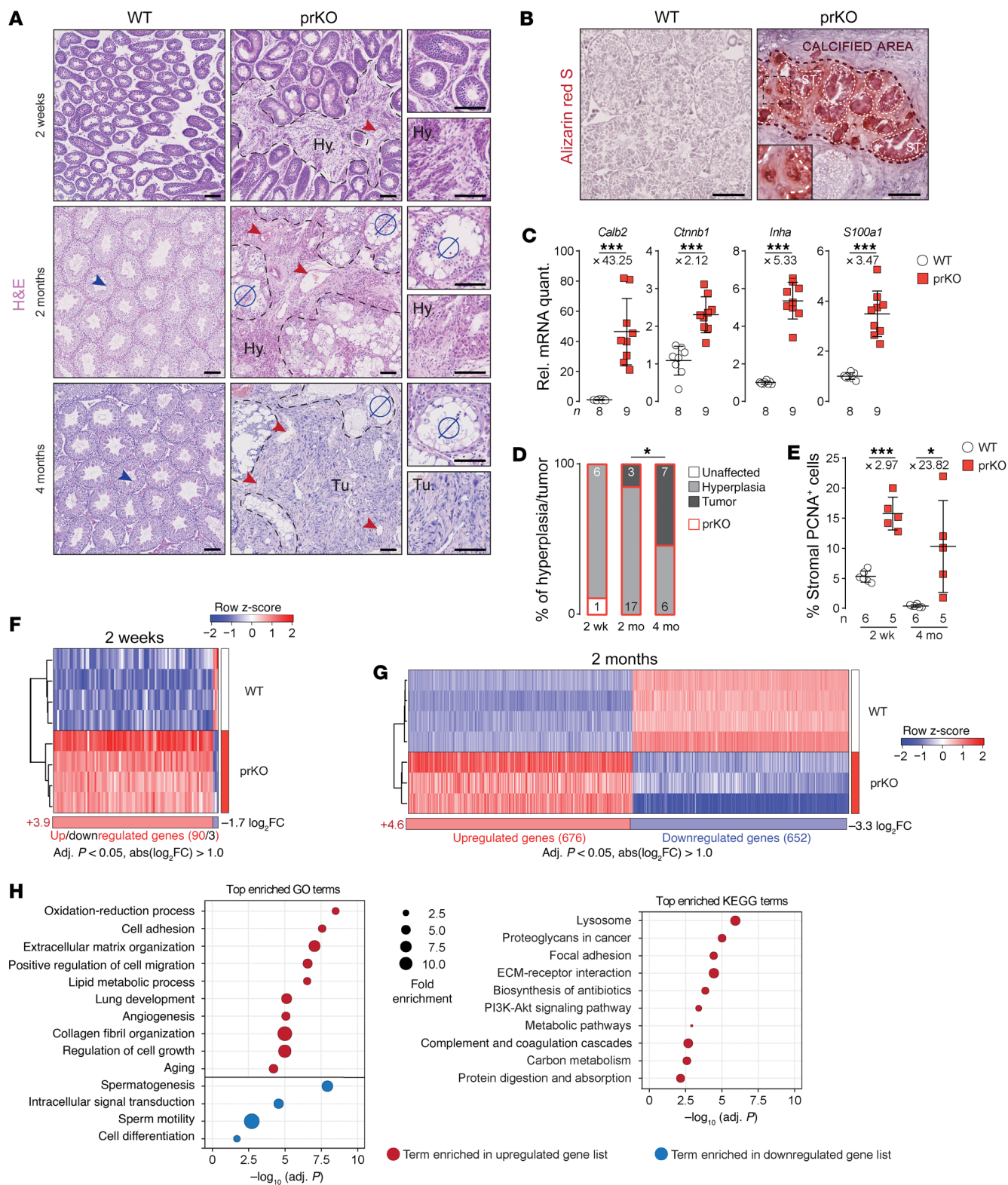
Figure 1. *Prkar1a* loss in mouse testicular somatic cells induces LCCSCTs-like lesions. (**A**) H&E staining of 2-week-old, 2-month-old, and 4-month-old WT and *Prkar1a* somatic progenitor cell KO testes (noted as prKO, *Sf1:Cre,Prkar1a*^{fl/fl}). Red arrowheads indicate prKO hypervascularization. Blue arrowheads indicate spermatozoa. Hy., hyperplasia; Tu., tumor; Ø, absence of spermatozoa. (**B**) Alizarin red S staining in 2-month-old prKO testis. Dashed lines delineate calcium accumulation areas in both ST and stroma (inset). (**C**) RT-qPCR analysis for LCCSCT marker transcripts (*Calb2, Ctnnb1, Inha, S100a1*) in 4-month-old WT and prKO testes. Statistical analysis was performed using Student's *t* test or Welch's *t* test. Rel, relative; quant, quantification. (**D**) Relative proportion of hyperplasia and tumor from 2-week-old to 4-month-old prKO testes evaluated following H&E staining. Number of each histological defect is indicated in bars. Statistical analysis was performed using 2-proportion Fisher's test (hyperplasia/tumor proportions between 2-month-old and 4-month-old prKO testes). $P = 0.0259$. (**E**) Stromal PCNA[+] cell quantification represented as percentages of cells in 2-week-old and 4-month-old WT and prKO testes. Statistical analysis was performed using Welch's *t* test. (**F** and **G**) Heatmap representing the median-centered expression of significantly deregulated genes (abs[log₂ FC > 1] and adj. $P < 0.05$) in 2-week-old (**F**) and 2-month-old (**G**) prKO testes ($n = 3$–4) compared with WT ($n = 4$). (**H**) Top 10 enriched GO and KEGG terms using 2-month-old prKO significant deregulated genes. Bars represent mean per group ± SD. Scale bars: 100 μm. Original magnification, ×2.12 (inset, **B**). *$P < 0.05$; ***$P < 0.001$.

tomic data from comparative lrKO versus WT testes microarray analyses confirmed fewer molecular deregulations in 2-month-old lrKO testes, with only 22 significantly deregulated genes (17 up- and 5 downregulated genes; Figure 2G). In contrast, loss of *Prkar1a* in SC (srKO model) was sufficient to reproduce intratubular and peritubular LCCSCT lesions and led to infertility (Figure 2, A–D, and Supplemental Figure 4, E and F). The unbiased transcriptomic analyses revealed a huge deregulation of the molecular networks in 2-month-old srKO testes (560 deregulated, 150 up- and 410 downregulated genes; Figure 2, F and G). Comparative heatmap analyses among WT, prKO, srKO, and lrKO model data highlighted a main cluster of 473 genes (84.4 % of srKO deregulated genes) exhibiting deregulations in both 2-month-old prKO and srKO mutant testes (114 up- and 359 downregulated genes) compared with WT. Consistent with the GC population decrease, 75.5% of these cluster genes were significantly downregulated and strongly associated with spermatogenesis alteration in gene set enrichment analyses (GSEA) (Figure 2, G and H, and Figure 3A). Unlike the prKO model, adult srKO mice had normal testosterone plasma levels and never developed tumors (up to 12 months of age; Supplemental Figure 4, G and H). In agreement with the delayed *Prkar1a* loss impact previously observed in the prKO model, transcriptomic analyses of both 2-week-old lrKO and srKO testes revealed very little divergence from WT molecular signatures (Figure 2F). Together, data from srKO mice demonstrated that SC-specific loss of *Prkar1a* failed to initiate tumorigenesis, although ST functions were altered.

PKA overactivation in SCs triggers increased GC apoptosis from prepubertal age. Adult prKO and srKO mice shared common deregulated molecular signatures associated with nonautonomous GC loss that could be attributed to disturbed SC nursing capacities. Hallmark GSEA showed a robust negative enrichment for a "spermatogenesis" gene set and a positive enrichment for an "apoptosis" gene set in srKO and prKO testes compared with WT (Figure

3, A and B, and Supplemental Data File 3). In order to specify the nature of the cellular events leading to the GC loss at adulthood in response to Sertoli *Prkar1a* inactivation, developing GC types in srKO testes were evaluated. Significantly increased TUNEL staining over the entire width of the germinal epithelium from 5-week-old and 2-month-old srKO testes confirmed that apoptosis induced by *Prkar1a* loss occurred at different spermatogenesis stages and contributed to decreases in germinal epithelium thickness (Figure 3, C–F). Although a complete lack of spermatozoa was evidenced in 2-month-old srKO ST (Figure 3G), immunostaining analyses only identified a significant 1.8-fold decrease in ZBTB16^{+} spermatogonia and a 1.6-fold decrease in G9A[+] cell numbers (Figure 3, H–K), corresponding to the undifferentiated spermatogonia up to early leptotene spermatocyte populations. Moreover, SYCP3^{+} spermatocyte numbers were unchanged in srKO compared with WT (Figure 3, L and M), suggesting the occurrence of compensatory events counteracting increased apoptotic GC counts. Indeed, further time-course analyses revealed a transient growing number of ZBTB16^{+} cells, G9A^{+} cells, and SYCP3^{+} meiotic cells from 2 up to 5 weeks of age, which paralleled a significant increased srKO testis weight from PND9 to 5 weeks compared with WT (Supplemental Figure 5, A and B). This enhanced germ-line expansion, including elongated spermatid formation, resulted in an abnormal overfilling of the srKO ST as attested by testis weight that culminated at 5 weeks of age before being drastically drained thereafter (Supplemental Figure 5, C–E). SOX9 immunostaining analyses revealed that SC numbers were significantly increased, 1.17-fold, in 2-week-old srKO testis compared with WT and 0.85-fold decreased at 7 weeks (Supplemental Figure 6, A and B). However, these slight variations were unlikely to fully account for the magnitude of the alterations affecting the germ line. Together, these data suggest that the lack of germ line in adult srKO testis was rather due to chronic apoptosis events overlapping with a deregulated increase of GC population instead of a meiosis commitment blockade in response to SC *Prkar1a* gene inactivation. These observations are consistent with DDX4 immunostaining in human CNC-LCCSCT biopsies, which reveal a strong decrease in GC numbers (Figure 3, N–P).

PKA overactivation alters SC polarity. The formation of vacuoles inside the germinal epithelium associated with round clusters of GCs that are released in the lumen was another phenomena, specifically occurring in the testes of CNC patients and prKO and srKO mice, that resulted, together with apoptosis, in the loss of spermatogenic cells (Supplemental Figure 7, A and B). Comparative time-course analyses of srKO and prKO histological intratubular alterations indicated a more precocious prKO increase in vacuolated tubules into the germinal epithelium compared with the srKO model that could contribute to worsen GC depletion (Supplemental Figure 7, A and D). Consistent with these observations, GSEA of the transcriptome of 2-month-old srKO testis revealed extended modification of the molecular networks supporting tubule architecture, including cytoskeleton, adhesion, or junctional proteins (Figure 4A). To gain insight into the modulators of the germinal epithelium integrity, we extracted expression levels of 32 genes involved in Sertoli-Sertoli junctions or Sertoli-GC interactions. Fifteen of these 32 genes were significantly upregulated, and 3 genes were downregulated both in srKO and prKO testes compared with WT (Figure 4B). RT–qPCR conduct-
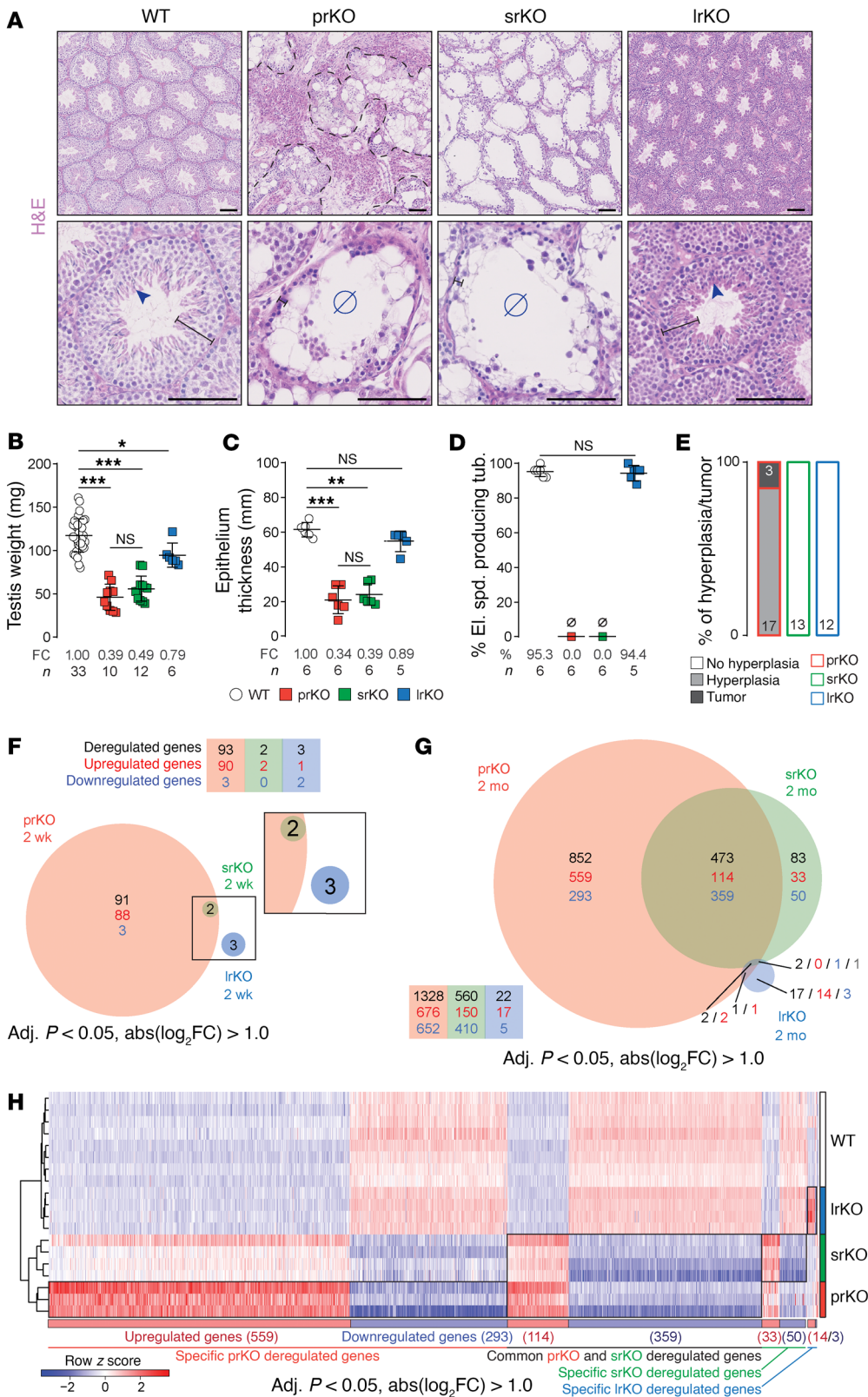
Figure 2. Seminiferous defects are associated with *Prkar1a* loss in SCs. (**A**) H&E staining of 2-month-old WT, prKO (*Sf1:Cre,Prkar1a*^fl/fl; somatic progenitor cell *Prkar1a* inactivation) (already presented in Figure 1A), srKO (*Amh:Cre,Prkar1a*^fl/fl; SC *Prkar1a* inactivation), and lrKO (*Cyp11a1:Cre,Prkar1a*^fl/fl; LC *Prkar1a* inactivation) testes. Dashed black lines delineate the tumor developed in prKO testis, blue arrowheads show spermatozoa, and black lines limit seminiferous epithelium thickness. Ø, absence of spermatozoa. Scale bars: 100 μm. (**B**) Testis weight of 4-month-old WT, prKO, srKO, and lrKO mice. One-way ANOVA was followed by Tukey's multiple-correction test. (**C**) Epithelium thickness quantified following H&E staining in 2-month-old WT, prKO, srKO, and lrKO testes. Kruskal-Wallis test was followed by Dunn's multiple-correction test. (**D**) Quantification of ST with elongated spermatids (el. spd.) represented as a percentage of positive tubules (tub.) quantified following H&E staining in 2-month-old WT, prKO, srKO, and lrKO testes. Statistical analysis was performed using Student's *t* test. (**E**) Relative proportion of hyperplasia and tumor in 2-month-old prKO, srKO, and lrKO testes. Numbers for each histological defect and genotype are indicated in bars. (**F** and **G**) Venn diagrams of the significantly deregulated genes (abs[log₂] FC > 1 and adj. *P* < 0.05) in 2-week-old (**F**) and 2-month-old (**G**) prKO, srKO, and lrKO testes compared with WT (*n* = 3–4 mice per group). (**H**) Heatmap representing the median-centered expression of significantly deregulated genes in 2-month-old prKO, srKO, and lrKO testes compared with WT. Bars represent the mean per group ± SD. *$P < 0.05$; **$P < 0.01$; ***$P < 0.001$.

ed on independent WT, srKO, and prKO samples confirmed these results (Supplemental Figure 7E). Immunohistological analyses of Claudin11 (*Cldn11*) and β-catenin (*Ctnnb1*) specified that these junction proteins involved in blood-testis barrier (BTB) establishment were delocalized to the entire membrane perimeter in both srKO and prKO mutant testes (5 weeks) and that β-catenin staining was also diffused into the cytoplasm (Figure 4, C–E). These delocalizations were associated with a SC cytoskeleton alteration attested by tubulin β3 densification and vimentin disorganization (Supplemental Figure 7F). The junctional defects were also
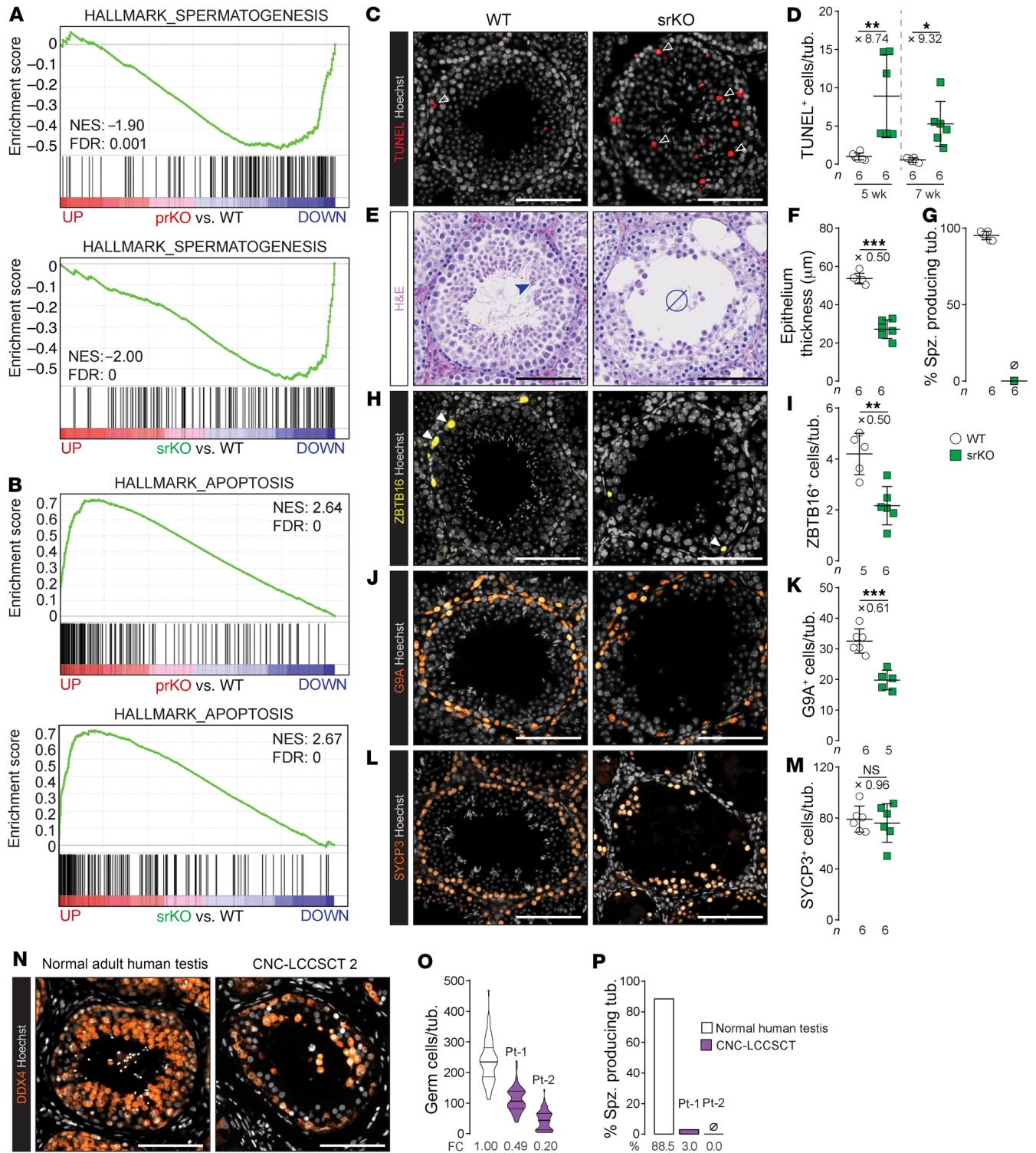
Figure 3. PKA overactivation in SCs triggers increased GC apoptosis from prepubertal age. (**A** and **B**) GSEA of microarray gene expression data of hallmark-spermatogenesis gene list (**A**) and hallmark-apoptosis gene list (**B**) in both 2-month-old prKO and srKO testes compared with WT. NES, normalized enrichment score. (**C**) TUNEL staining in 5-week-old WT and srKO testes. White open arrowheads indicate TUNEL+ cells. (**D**) Quantification of TUNEL+ cells in 5-week-old and 7-week-old srKO testes compared with WT. Statistical analysis was performed using Welch's *t* test or Mann-Whitney *U* test. (**E**) H&E staining of 7-week-old WT and srKO testes. Blue arrowhead indicates spermatozoa; Ø indicates absence of spermatozoa. (**F** and **G**) Epithelium thickness quantification (**F**) and percentage of ST with elongated spermatids (**G**) in 7-week-old WT and srKO testes. Statistical analysis was performed using Student's *t* test. (**H**–**M**) Immunohistochemical detection and quantification of ZBTB16 (spermatogonia-A) (**H** and **I**), G9A (spermatogonia-B) (**J** and **K**), and SYCP3 (spermatocytes) (**L** and **M**) in 7-week-old WT and srKO testes. Quantification is based on the number of positive cells per tubule. Statistical analysis was performed using Student's *t* test. (**N** and **O**) DDX4 immunohistochemical detection (**N**) and GC loss quantification in CNC-LCCSCTs compared with normal adult human testis (**O**). (**P**) Percentages of ST with elongated spermatids quantified following H&E staining in CNC-LCCSCTs compared with normal adult human testis. Bars represent the mean per group ± SD. Scale bars: 100 μm. *$P < 0.05$; **$P < 0.01$; ***$P < 0.001$.
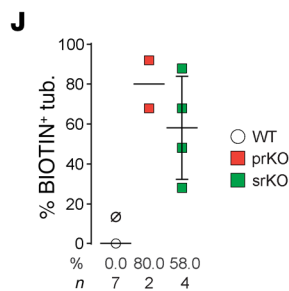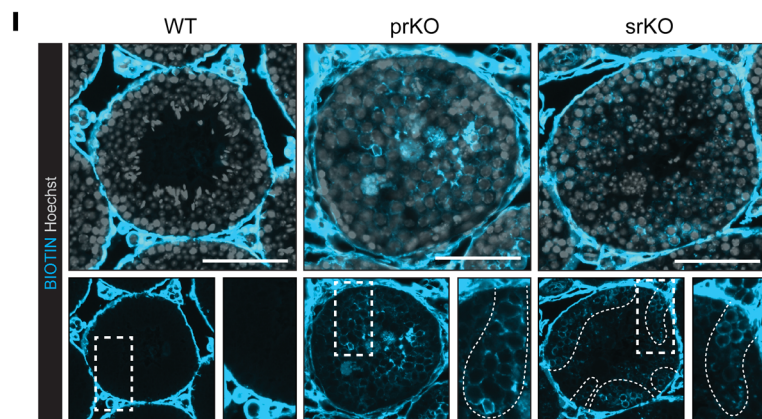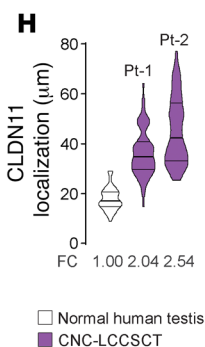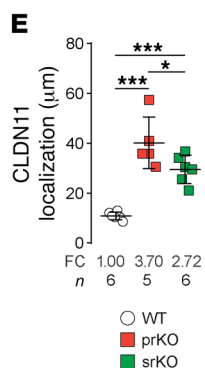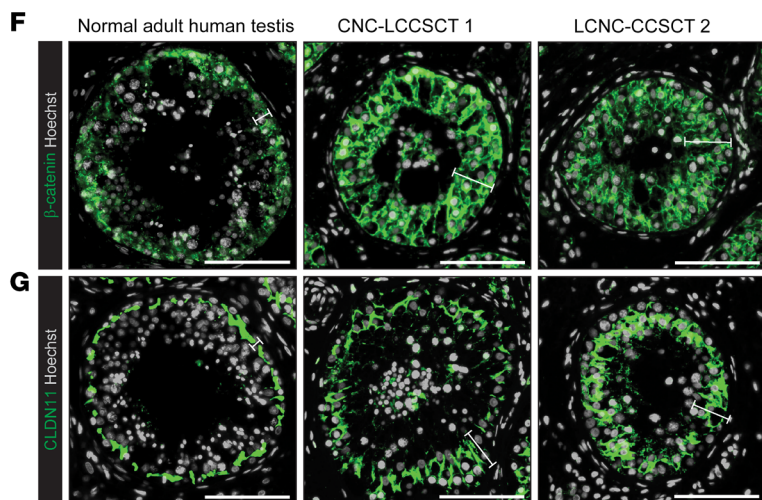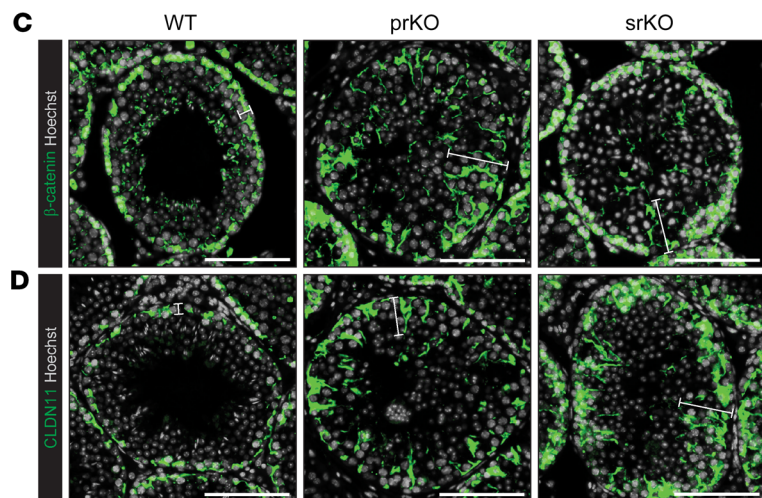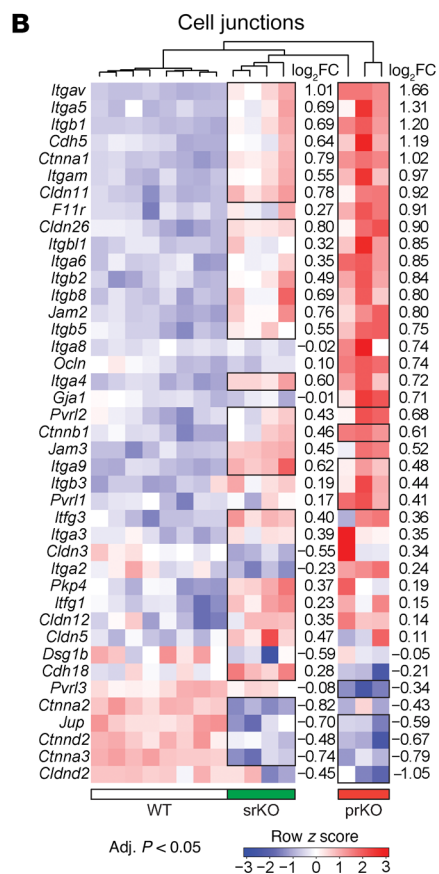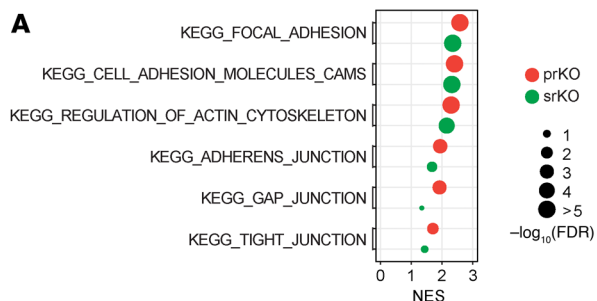
Figure 4. PKA overactivation alters SC polarity. (A) GSEA enrichment scores of microarray gene expression data using KEGG gene lists associated with junction/cytoskeleton in 2-month-old prKO or srKO testes compared with WT. **(B)** Heatmap representing the median centered expression of significantly deregulated regulators of cell junctions (for black boxes, adj. $P < 0.05$) in 2-month-old prKO and srKO testes ($n = 3–4$) compared with WT ($n = 4$). **(C–H)** Immunohistochemical detection of β-catenin and CLDN11 and quantification of CLDN11 expression domain based on the distance between basal lamina and apical CLDN11 in 5-week-old WT, prKO, and srKO testes and in normal adult human testis and CNC-LCCSCTs. White lines delineate β-catenin or CLDN11 expression domain. One-way ANOVA was followed by Tukey's multiple-correction test. **(I)** Biotin tracer detection after injection underneath the testis capsule in 6-week-old WT, prKO, and srKO testes. White dashed lines mark intraseminiferous biotin diffusion in prKO and srKO testes. **(J)** BTB integrity loss evaluation based on the percentage of tubule with intraseminiferous biotin accumulation. Scale bars: 100 μm. *$P < 0.05$; ***$P < 0.001$.

present in the human CNC ST located out of the tumor mass, as attested by Claudin11 and β-catenin IHC analyses (Figure 4, F–H). These data suggested a compromised setting of the adluminal compartment by the BTB junctions, which is critical to spermatogenesis achievement (24). Therefore, BTB functional integrity was tested in the srKO and prKO mutant mice by intratesticular injection of a fluorescent tracker (Figure 4, I and J). The tracker signal confirmed a drastic loss of BTB sealing in both srKO and prKO (6 weeks of age), demonstrating that SC failed to provide an appropriate structural dynamic for GC maturation across the seminiferous epithelium. Moreover, transcriptomic and RT-qPCR analyses highlighted an upregulation of *Dpt* expression in 2-week-old prKO and in 2-month-old srKO and prKO testes (Supplemental Figure 7G), indicating increased dermatopontin production by both altered adult STs and the hyperplastic stromal compartment. Our results are consistent with previous data demonstrating that the dermatopontin excessive production in SCs induced BTB alterations, vacuole formation, and GC loss (25). However, srKO and prKO comparative analyses also revealed precocious and higher growing *Dpt* transcript levels associated with tumor expansion in prKO testes. These latest observations are consistent with previous data highlighting cAMP controlled expression of *Dpt* and its involvement in tumor growth (26, 27).

PKA overactivation modifies Sertoli signals involved in the control of spermatogenesis. The maintenance of GCs within the spermatogenic cycle is supported by mature SCs through appropriate production of mitogens and differentiation factors that could be affected by *Prkar1a* gene inactivation. The interaction of the growth factor Kit-ligand (KIT-L) produced by SCs with its specific c-KIT receptor expressed on GCs from differentiating spermatogonia causes the PI3K-AKT pathway activation that is required for proliferation and survival of mitotic GCs in both the embryonic and postnatal testes (28–30). KIT-L also triggers PI3K/AKT and Ras/MAPK crosstalk that plays a critical role in the development of GC cancers (31). In addition, the KIT-L/c-KIT/JAK/STAT pathway is the main promoter of mast cell growth and differentiation from bone marrow and peripheral progenitors (32). Cyclic AMP/PKA-driven mechanisms leading to increased *Kitl* transcription in SCs have been previously described (33, 34). Consistent with these previous observations, transcriptomic and RT-qPCR analyses in

prKO/srKO testes showed that *Prkar1a* loss led to a significant and early upregulation of *Kitl* transcripts associated with a positive enrichment of Reactome signaling by the SCF (alias KIT-L)/KIT gene set as well as an increase in mast cell recruitment in interstitial tissue (Figure 5, A–D).

Surprisingly, further transcriptomic and RT-qPCR analyses highlighted a significant upregulation of *Wnt4* gene expression that was listed in the common deregulated gene cluster from adult prKO and srKO models, indicating that most of the WNT4 overproduction originated from adult SCs in response to *Prkar1a* inactivation (Figure 5, E and F). Heatmap of a WNT signaling gene set showed a robust positive enrichment of these molecular signatures in adult srKO and prKO testes compared with WT, suggesting a functional significance of WNT pathway activation. This observation was confirmed by RT-qPCR analysis of *Axin2*, *c-Myc*, *Ccdc80*, and *Nr0b1* target gene expression (Figure 5G and refs. 35, 36). Together, these data reveal that constitutive PKA activation leads to upregulation of *Wnt4* in SCs, whereas PKA-dependent *Wnt4* gene expression was only previously demonstrated in other tissue differentiations, such as kidney tubulogenesis or uterine stromal cell decidualization (37, 38).

Wnt4 inactivation decreases GC apoptosis induced by Prkar1a loss. The WNT4/β-catenin pathway is involved in stem cell proliferation of several tissues (39). Although WNT4/β-catenin has been shown to be an essential modulator of female ovary differentiation (40), *Ctnnb1* expression is dispensable for testis development (41). Moreover, Boyer et al. demonstrated that an excessive WNT4 signal repressed the normal activity of spermatogonial stem cells by inducing their apoptosis (42), while forced expression of active β-catenin in fetal gonocytes deregulated spermatogonial proliferation and apoptosis (43, 44). Our analyses indicated that the increase in GC apoptosis together with disturbed BTB establishment impaired the spermatozoa accumulation in prKO and srKO mice. In order to assess the role of WNT4 in GC-altered homeostasis triggered by *Prkar1a* gene loss, we generated double-KO mice for *Prkar1a* and *Wnt4* in somatic cells (prwKO model; *Sf1:Cre,Prkar1a*$^{fl/fl}$,*Wnt4*$^{fl/fl}$) or restricted to SCs (srwKO model; *Amh:Cre,Prkar1a*$^{fl/fl}$, *Wnt4*$^{fl/fl}$; Supplemental Figure 8, A–D). As expected, simple mutant mice bearing targeted *Wnt4* inactivation in SC (swKO) or in somatic cells (pwKO) were fertile and had normal testicular development and physiology (Supplemental Figure 8E). Unlike the srKO testis, ST from 8-week-old double-mutant srwKO testes maintained a complete germinal epithelium containing all GC types, including spermatozoa and were associated with a significant decrease in intratubular apoptosis events compared with srKO testes (Figure 6, A–J). This indicates that *Wnt4* loss in a PKA activation context allowed the achievement of a complete GC lineage, whereas SC junction disorganization, vacuole, and infertility were still maintained (Figure 6, J–M). Therefore, SC-specific PKA constitutive activity upregulated *Wnt4* expression, which increased GC apoptosis. Nevertheless, several spermatocytes with abnormal mitotic features not only persisted in srwKO, but also were accentuated in prwKO testes, despite normalization of the germ-line marker gene *Ddx4* (Figure 6A and Supplemental Figure 8F). These data revealed a critical role of SC-specific PKA signaling on spermatogenesis that impaired long-term maintenance of GCs, which is independent of the WNT4 signal. Transcriptomic and RT-qPCR analyses highlighted increased *Ctnnb1*
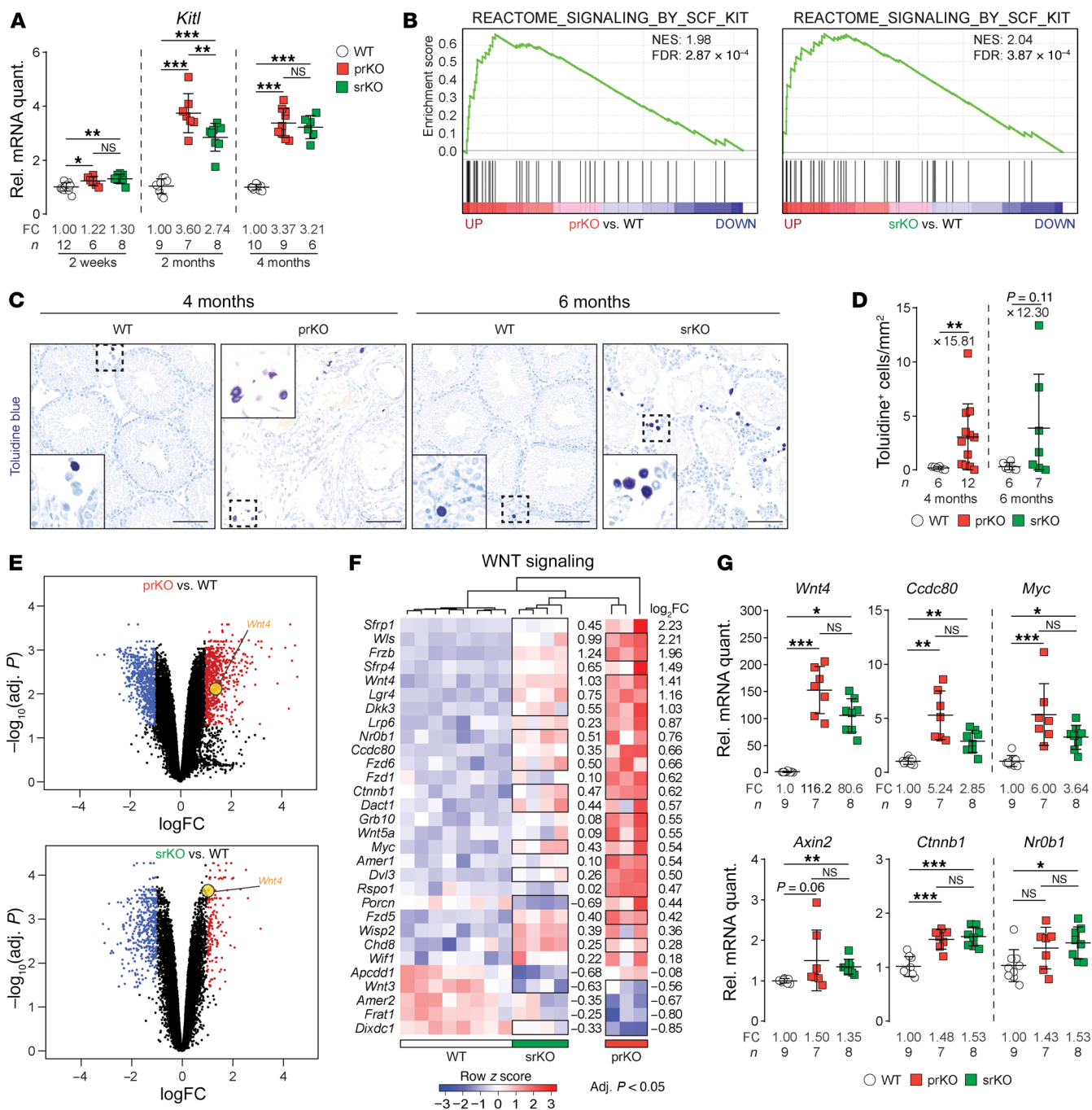
Figure 5. PKA overactivation modifies Sertoli signals involved in control of spermatogenesis. (**A**) *Kitl* transcripts of RT-qPCR analysis in 2-week-old, 2-month-old, and 4-month-old WT, prKO, and srKO testes. One-way ANOVA was followed by Tukey's multiple-correction test, and Welch's 1-way ANOVA was followed by Games-Howell multiple-correction test. (**B**) GSEA of microarray gene expression data using Reactome signaling by the SCF KIT gene list in 2-month-old prKO and srKO testes compared with WT. (**C**) Toluidine blue staining showing mast cell recruitment in 4-month-old prKO and 6-month-old srKO testes. Scale bars: 100 μm. Original magnification, ×2.65 (insets, **C**). (**D**) Mast cell quantification based on the toluidine[+] cell number per histological section. Statistical analysis was performed using Welch's *t* test. (**E**) Volcano plot showing differential gene expression in 2-month-old prKO and srKO testes compared with WT. Significantly deregulated genes (abs[log₂ FC > 1 and adj. *P* < 0.05) are highlighted in blue (down) or in red (up). *Wnt4* (yellow point) is an upregulated gene. (**F**) Heatmap representing the median centered expression of significantly deregulated WNT pathway regulators and target genes (for black boxes, adj. *P* < 0.05) in 2-month-old prKO and srKO testes (*n* = 3-4) compared with WT (*n* = 4). (**G**) RT-qPCR analysis of WNT pathway regulators (*Wnt4*, *Ctnnb1*) and target gene (*Axin2*, *Ccdc80*, *Myc*, *Nr0b1*) expression in 2-month-old WT, prKO, and srKO testes. One-way ANOVA was followed by Tukey's multiple-correction test, Welch's 1-way ANOVA was followed by Games-Howell multiple-correction test, and Kruskal-Wallis test was followed by Dunn's multiple-correction test. Bars represent the mean per group ± SD. **P* < 0.05; ***P* < 0.01; ****P* < 0.001.
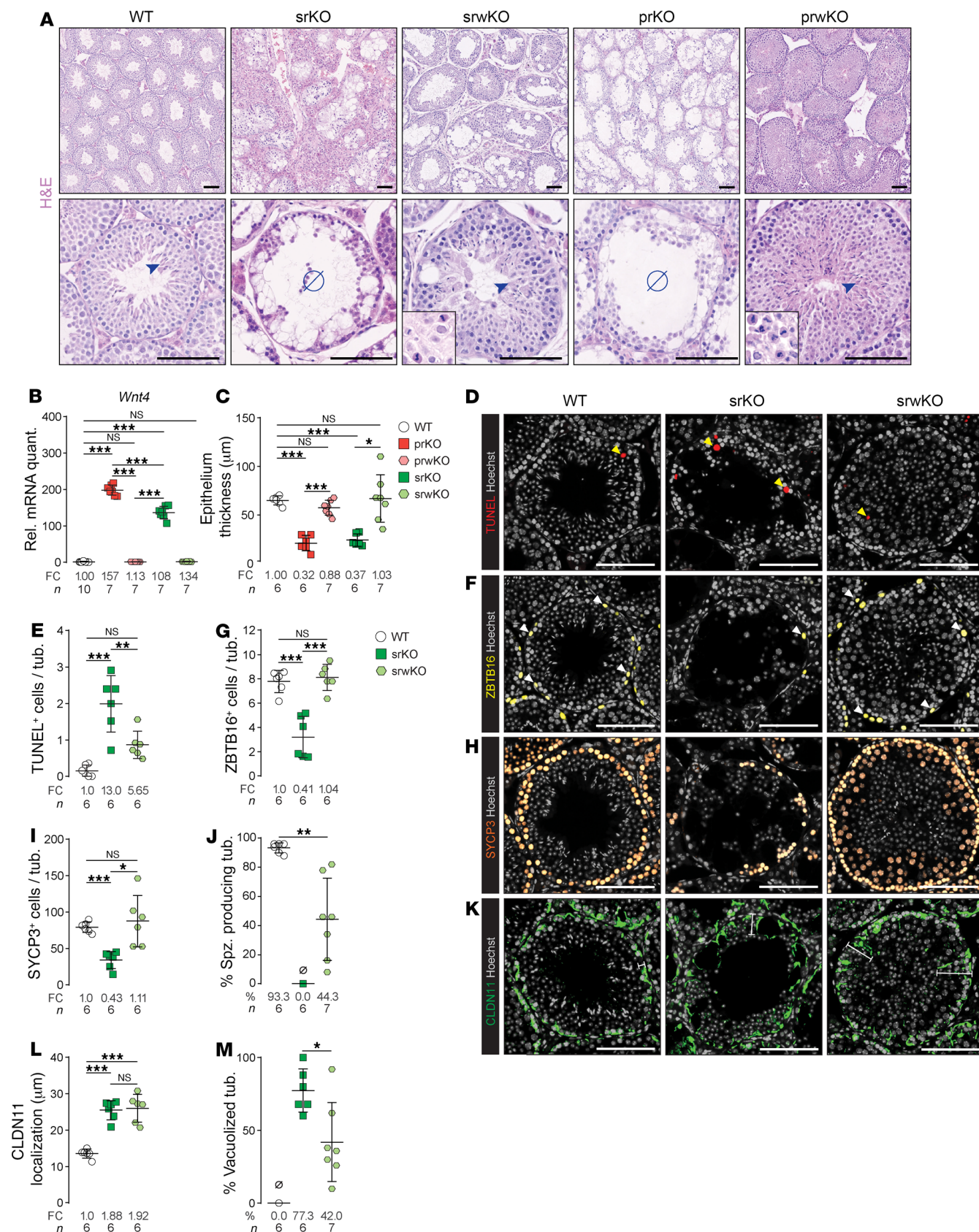
Figure 6. *Wnt4* inactivation decreases GC apoptosis induced by *Prkar1a* loss. (**A**) H&E staining of 2-month-old WT, prKO, double-mutant prwKO testes (*Sf1:Cre,Prkar1a^fl/fl^,Wnt4^fl/fl^*), and srKO and srwKO testes (*Amh:Cre,Prkar1a^fl/fl^,Wnt4^fl/fl^*). Arrowheads indicate spermatozoa; Ø indicates absence of spermatozoa; insets show abnormal mitotic features. (**B**) RT-qPCR analysis of *Wnt4* transcripts in 2-month-old WT, prKO, prwKO, srKO, and srwKO testes. Welch's 1-way ANOVA was followed by Games-Howell multiple-correction test. (**C**) Epithelium thickness quantified following H&E staining in 2-month-old WT, prKO, prwKO, srKO, and srwKO testes. Welch's 1-way ANOVA was followed by Games-Howell multiple-correction test. (**D** and **E**) TUNEL staining in 2-month-old WT, srKO, and srwKO testes (**D**) and TUNEL⁺ cell quantification (**E**) in 2-month-old srwKO testes compared with WT and srKO testes. Yellow arrowheads indicate TUNEL⁺ cells. One-way ANOVA was followed by Tukey's multiple-correction test. (**F–I**) Immunohistochemical detection of ZBTB16 (**F**) and SYCP3 (**H**) in 2-month-old WT, srKO, and srwKO testes and quantification of ZBTB16 (**G**) and SYCP3 (**I**) based on the number of positive cells per tubule. White arrowheads indicate ZBTB16⁺ cells. Welch's 1-way ANOVA was followed by Games-Howell multiple-correction test. (**J**) Percentage of ST with elongated spermatids quantified following H&E staining in 2-month-old WT, srKO, and srwKO testes. Statistical analysis was performed by Welch's *t* test. (**K**) Immunohistochemical detection of CLDN11 in 2-month-old WT, srKO, and srwKO testes. (**L** and **M**) Quantification of CLDN11 expression domain (**L**) and percentage of vacuolized tubules (**M**) in 2-month-old srwKO testis compared with WT and srKO. Statistical analysis was performed using Student's *t* test or 1-way ANOVA followed by Tukey's multiple-correction test. Bars represent the mean per group ± SD. Scale bars: 100 μm. Original magnification, ×1.41. (insets, **A**). *$P < 0.05$; **$P < 0.01$; ***$P < 0.001$.

mRNA levels in the adult testes of both prKO and srKO mice, which remained elevated in srwKO and prwKO (Supplemental Figure 8G), demonstrating that PKA induced *Ctnnb1* expression independently of the WNT4 signal.

Wnt4 inactivation impaired tumor mass formation induced by Prkar1a loss. Human CNC-LCCSCT masses are the site of proliferative activity mediated by molecular pathways that, to our knowledge, had not been identified until now. Consistent with LCCSCTs in the CNC context, from 8 weeks of age, prKO testis developed early proliferative tumor masses arising from neonatal stromal hyperplasia. RT-qPCR and IHC analyses highlighted an upregulation of *Wnt4* and *Ctnnb1* expression in 2-month-old prKO mice, suggesting, together with the WNT-signaling heatmap analysis (Figure 5, F and G, and Supplemental Figure 8, C and D), that PKA-induced WNT/β-catenin signaling could be involved in the LCCSCT promotion in CNC patients and prKO mice. In addition to *Wnt4* upregulation, further analyses indicated that the loss of *Prkar1a* led to a chronic increase of both active β-catenin accumulation and gene expression of *Fzd6* and *Wnt5a* in 4-month-old prKO testes (Figure 5F and Figure 7, A–C). Interestingly, increased expression of *Fzd6* and *Wnt5a* were previously associated with tumor expansion through canonical and noncanonical WNT pathway activity in various cancers (45). Histological examination of mutant testes revealed that, although the oldest double-mutant prwKO testes were still the site of stromal fibrosis, they were devoid of tumors compared with single-mutant prKO testes (Figure 7, D–F, and Supplemental Figure 8E). Comparative PCNA IHC analyses confirmed that *Wnt4* inactivation strongly decreased the stromal proliferation that was triggered by *Prkar1a* loss in somatic testis cells (Figure 7, G and H). Moreover, whole-testis

RT-qPCR analyses confirmed that in these prwKO testes, *Ccdc80*, *Axin2*, and *Ki67* transcripts were reduced compared with those in 4-month-old prKO testes (Figure 7, I and J). Together, these results demonstrate that WNT4 is a testis tumor signal in response to *Prkar1a* inactivation. Consistent with our murine models, IHC analyses confirmed that human CNC-LCCSCT cells retained WNT4 staining that colocalized with cytoplasmic β-catenin accumulation. This demonstrates that WNT/β-catenin activation is likely associated with human CNC-LCCSCT expansion (Figure 7K).

PKA constitutive activation in somatic cells activates growth factor signaling pathways in CNC-LCCSCTs. Unbiased GO and GSEA highlighted additional prKO-specific enrichment in signatures associated with proliferative pathways that could participate in tumor formation, including upregulated expression for *Fgf2*, *Egf*, *Igf1*, and *Tgfb1-3* (Figure 8, A–D). These increased *Fgf2*, *Egf*, *Igf1*, and *Tgfb1-3* transcript levels in prKO testes remained unaffected by *Wnt4* loss, suggesting that their PKA-induced upregulation was not sufficient to trigger precocious tumor formation (Figure 8E). Proliferative/oncogenic activities of the growth factors (IGF1, EGF, FGF2, KIT-L) overexpressed in prKO testes are mainly mediated by converging signaling pathways, including RAS/MAPK and PI3K/AKT/mTOR (46–49). Immunodetection of activated MAPK modulators and mTOR targets in Western blot revealed significantly increased levels of phosphorylated forms of ERK, 4EBP1, and S6K in 4-month-old prKO testes compared with WT (Figure 8, F and G). These increases persisted after *Wnt4* inactivation in the 4-month-old prwKO testes, revealing that the loss of *Wnt4* did not affect the p4EBP1, pERK, and pS6K relative protein levels compared with their respective increased levels in *Prkar1a*-KO testes. In testis, the mTOR pathway was previously shown to control SC polarity and spermatogenesis (50, 51). Additionally, its overactivity was demonstrated to mediate SC disruption in a mouse model lacking the *Lkb1* gene in SCs (52). In prKO testes, IHC analyses revealed increased p4EBP1 accumulation in the tubular compartment and tumor mass compared with WT, demonstrating that the mTOR pathway was activated in tumor cells in response to *Prkar1a* loss (Figure 8H). Consistent with these observations, IHC analyses revealed that the human LCCSCT samples retained strong p4EBP1 immunostaining restricted to the majority of tumor cells and absent from nontumor areas (Figure 8I). Moreover, to a lesser extent, the human LCCSCT masses also displayed numerous foci of pERK accumulation, demonstrating that these 2 proliferative pathways are activated in CNC-LCCSCTs in response to *PRKAR1A* inactivation (Figure 8J). LCCSCTs are solid tumors; this implies they could be the site of hypoxia. This hypothesis was strongly suggested in 2-month-old prKO testes by GO and GSEA analyses highlighting positive enrichment in hypoxia-responsive genes (Figure 8, A and K). RT-qPCR analyses in 4-month-old prKO mice confirmed increased mRNA levels of *Hif1a*, *Hif1b*, and *Hif2a* genes that played a central role in O_2-dependent transcriptional response (Figure 8L). Consistent with these observations, IHC analyses in human LCCSCTs revealed increased cytoplasmic and nuclear HIF2A protein accumulation restricted to tumor cells (Figure 8M). Together, our data reveal that LCCSCTs are the site of multiple proliferative pathways, including mTOR, MAPK, and hypoxia, acting with the active WNT/β-catenin pathway to promote tumor growth.
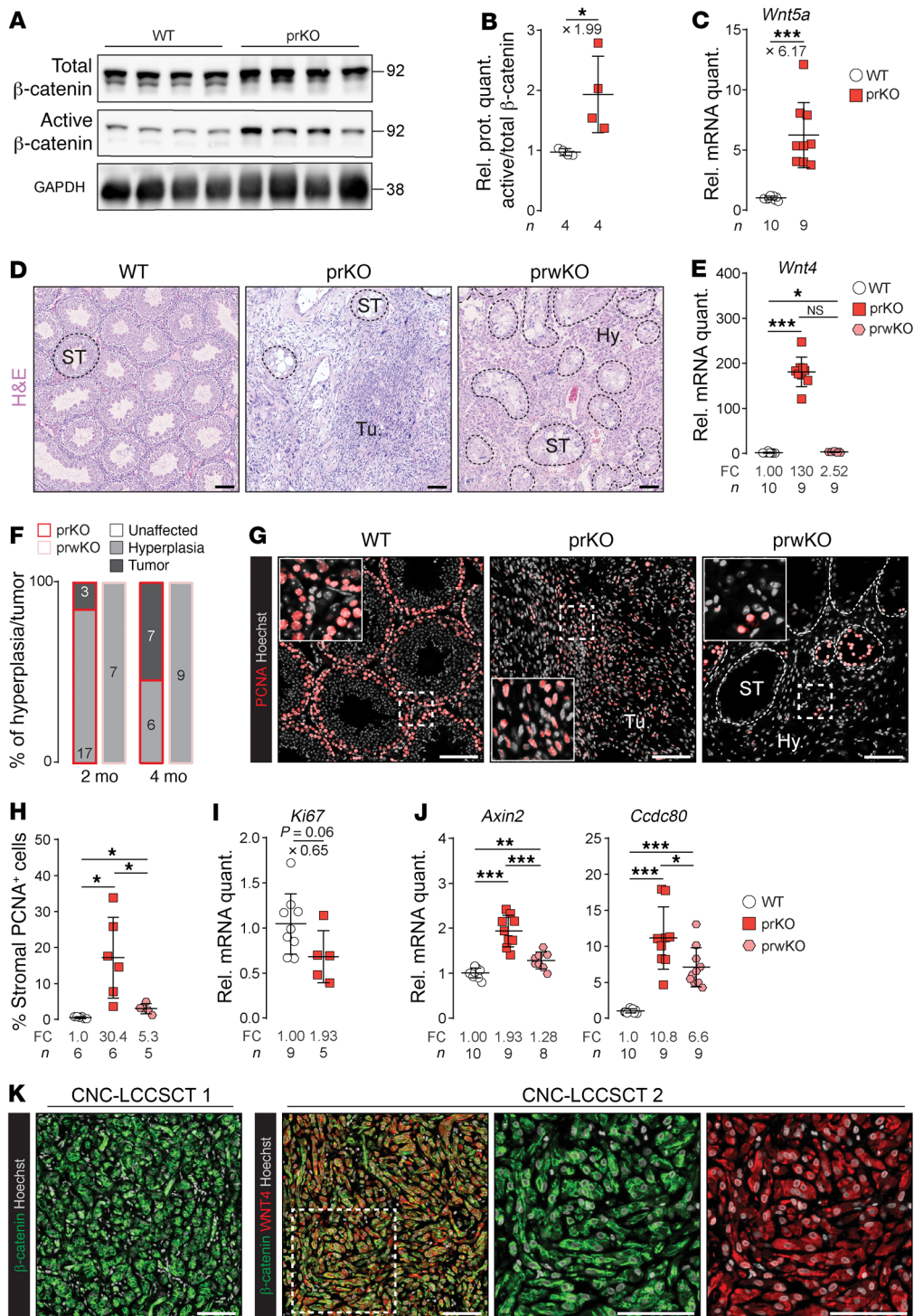
Figure 7. *Wnt4* inactivation impairs tumor mass formation induced by *Prkar1a* loss. (**A**) Active β-catenin accumulation in 4-month-old WT and prKO testes. (**B**) Active β-catenin quantification over total β-catenin. Statistical analysis was performed using Student's *t* test. prot., protein.(**C**) *Wnt5a* transcripts in 4-month-old WT and prKO testes. Statistical analysis was performed using Welch's *t* test. (**D**) H&E staining of 4-month-old WT, prKO, and prwKO testes. Dashed lines delineate ST. (**E**) *Wnt4* transcripts in 4-month-old WT, prKO, and prwKO testes. One-way ANOVA was followed by Tukey's multiple-correction test. (**F**) Relative proportion of testicular hyperplasia and tumor in 2-month-old and 4-month-old prKO and prwKO testes was evaluated following H&E staining. Numbers for each histological defect and genotype are indicated in bars. (**G**) Immunohistochemical analysis of PCNA in 4-month-old WT, prKO, and prwKO testes. (**H**) Quantification of stromal PCNA+ cells represented as a percentage of cells in 4-month-old WT, prKO, and prwKO testes. Welch's 1-way ANOVA was followed by Games-Howell multiple-correction test. (**I**) *Ki67* transcripts of RT-qPCR analysis in 4-month-old prKO and prwKO testes. Statistical analysis was performed using Student's *t* test. (**J**) *Axin2* and *Ccdc80* transcripts of RT-qPCR analysis in 4-month-old WT, prKO, and prwKO testes. One-way ANOVA was followed by Tukey's multiple-correction test, and Welch's 1-way ANOVA was followed by Games-Howell multiple-correction test. (**K**) Coimmunostaining for β-catenin and WNT4 in CNC-LCCSCTs. Bars represent the mean per group ± SD. Scale bars: 100 μm. Original magnification, ×2.65 (insets, **G**); ×2.00 (insets, **K**). *$P <$ 0.05; **$P <$ 0.01; ***$P <$ 0.001.

Discussion

To gain a better understanding of CNC-LCCSCT pathogenesis, we performed *Prkar1a* inactivation either targeted in the entire somatic compartment or in main subtypes of testicular somatic cells in mice. These unique mouse models, offering a more homogeneous sampling than human biopsies, provide access to early stages of pathology as well as advanced stages of tumor development. In addition, they constitute invaluable tools for deciphering crosstalks between deregulated molecular circuits.

The prKO mice develop all the alterations identified in CNC-LCCSCT patients (bilateral tumors arranged in solid cords, fibrosis, and calcifications associated with the increased expression of sex cord tumor markers [*Calb2*, *Ctnnb1*, *Inha*, and *S100*]), and therefore, they constitute a reliable model for exhaustive analyses of the molecular alterations caused by lack of the R1α subunit.

The ontogenetic analysis of the prKO model showed that major changes in endocrine activities, histological features, and the testicular transcriptome did not appear before the prepubertal stage; thus

they occurred with a delay compared with early fetal inactivation of the *Prkar1a* gene. This suggests that lack of the R1α subunit has little impact on testicular ontogeny during the fetal and perinatal periods. Conversely, in the princeps CNC mouse model carrying a constitutive homozygous *Prkar1a* deletion, lethality occurred as early as E8.5 due to growth defects in mesoderm-derived cardiac tissues, which can be rescued by further inactivation of the *Prkaca* gene encoding the Cα catalytic subunit of PKA (10). Possible compensatory mechanisms involving other PKA regulatory subunits, PKA inhibitor peptides, or phosphodiesterases in the developing fetal prKO testis remain to be determined. It should be noted that, although the occurrence of LCCSCTs in CNC patients may be observed as early as the first decade (5, 6, 53), no cases of testicular abnormalities have been reported at birth, suggesting that in humans, as in our mouse models, the *Prkar1a* mutation does not cause abnormal fetal gonadal development. In our models, the total absence of tumors in the double-mutant testis *Sf1:Cre,Prkar1a^{fl/fl}, Prkaca^{+/−}* demonstrates that the induction of testicular lesions of prKO mice relies on the unrepressed catalytic activity of PKA rather than on a defect of the R1α subunit per se, in agreement with previous observations in other tissue lesions of the CNC (9, 54, 55). The prKO testes transcriptomic analysis revealed a modified expression profile for more than 1328 genes in the 2-month-old testis associated with tissue and functional homeostasis disruption, which reflects the complexity of the mechanisms resulting from *Prkar1a* loss in all gonadal somatic cells. In addition, molecular signatures and histological analyses revealed germ-line damages resulting from paracrine/nonautonomous cell actions. Very few studies have looked at the infertilities associated with *PRKAR1A* mutations in CNC patients; nevertheless, previous studies showed alterations in male GCs (55, 56) as a consequence of *PRKAR1A* loss in somatic cells and GCs. The comparison of gene signatures of prKO testis with those of lrKO and srKO models allowed for demonstration that *Prkar1a* inactivation restricted to SCs led to a progressive germ-line loss from the prepubertal stages, resulting in infertility at puberty. In both prKO and srKO STs, the underlying mechanisms include an increase in GC apoptosis and formation of GC syncytia containing vacuoles reminiscent of those observed at the LCCSCT periphery in CNC patients. The massive apoptosis and desquamation mask the exacerbated increase in germ population that occurs in the first spermatogenesis waves in srKO testis compared with littermate control mice. These apoptotic events differ from the phenotypes observed in mouse models bearing FSH-R signaling upregulation (tgFSH/hpg and MT-hFSH-R mice) in which, at best, only an enhancement of spermatogonia proliferation and meiotic/postmeiotic cell survival was observed (57, 58). Likewise, the activating mutations of FSH signaling described in human species do not affect the fertility of male patients (59, 60). Notably, an activating mutation of the FSH-R has been shown to autonomously sustain spermatogenesis in a hypophysectomized man, and this has been further validated in mouse models (61, 62). While it is well documented that the FSH/FSH-R/PKA pathway exerts its effects on the germ line via the production of SC growth signals, such as FGF2, GDNF, or KIT-L (33, 34, 63–67), our data indicate that constitutive activation of PKA in the SC triggers additional circuits that oppose actions normally arising from FSH/FSH-R signaling. Indeed, the transcriptomic analysis of prKO and srKO testes allowed us to point

out a very strong WNT4 signal overproduction by mutant SCs. This observation is reminiscent of a previously described mouse model showing that SC-specific β-catenin constitutive activation leads to WNT4 overproduction and a subsequent decrease in the spermatogonial stem cell activity responsible for apoptosis and loss of GCs (42). In a report analyzing the testis of *E2f1-Wnt4* double-KO mice, Jorgez et al. specified that germ-line maintenance was dependent on *Wnt4* repression by *E2f1*, supporting a role of *Wnt4* in GC survival (68). Interestingly, in response to *Prkar1a* inactivation, our models also show WNT/β-catenin activation attested by upregulation of *Wnt4* and *Ctnnb1* expression and by increased accumulation of the β-catenin active form (i.e., dephosphorylated). In CNC patients, we also observed intracytoplasmic accumulation of β-catenin in SCs from testicular biopsies. Moreover, we found that about 36% of the genes upregulated in SCs from the *Ctnnb1^{tm1Mmt/+}; Amhr2^{tm3(cre)Bhr/+}* model (42) are also upregulated in srKO testis, indicating the establishment of partially common molecular alterations resulting from the mobilization of the WNT/β-catenin signaling pathway in the two models. Finally, by suppressing germ-line apoptosis in srwKO mice via *Wnt4* inactivation, we confirmed the hypothesis of a converging phenotype between these different mutant models and demonstrated the cooperation between overactive PKA and WNT/β-catenin signaling in triggering germ-line alterations. However, unlike the observations of Boyer and colleagues, our analyses of prKO and srKO mutants indicate that PKA-induced *Wnt4* upregulation is not associated with acquisition of the granulosa *Fst* marker. Moreover, SCs maintain high *Sox9* expression, while both *Foxl2* and *Rspo1* expression are absent from all *Prkar1a* mutant testis (42). Together, the comparison of *Ctnnb1^{tm1Mmt/+};Amhr2^{tm3(cre)Bhr/+}* and prKO or srKO models suggests that constitutive activation of PKA both triggers massive overexpression of *Wnt4* and opposes the *Wnt4* female identity programming function, possibly by reinforcing the maintenance of protesticular factors such as SOX9, which regulates its own expression and represses *Foxl2* expression (16, 69–72). Transcriptomic and IHC analyses reveal an increased production of the BTB proteins and SC-associated cytoskeleton components in both mutant murine and CNC human STs. These junctional proteins are known to be positively controlled by various factors, including SOX9 and also the androgen and mTOR-signaling pathways, both of which are enhanced in our models (51, 69, 73). However, an alteration of GC progression into the adluminal tubular compartment due to paracellular extension of SC BTB proteins is unlikely to contribute to GC apoptosis in *PRKAR1A*/*Prkar1a* mutant human and murine testes. Indeed, in double-mutant prwKO STs, the extended distribution of BTB proteins persists, while the GC apoptosis blockade partially restores the accumulation of elongated spermatids. This indicates that structural changes in the BTB induced by *Prkar1a* loss are mostly independent of WNT4 action and do not prevent spermatogenesis. Nevertheless, the SC nuclei delocalization and BTB functional failure are loss of polarity criteria suggestive of SC maturity disturbance in the srKO and prKO testes. However, unlike in the *Ctnnb1^{tm1Mmt/+}; Amhr2^{tm3(cre)Bhr/+}* model (74), in srKO and prKO STs, SCs do not proliferate and no overproduction of AMH persists at adulthood. These data indicate that activation of PKA in SCs induces specific prodifferentiating actions that counteract some exacerbated effects of WNT/β-catenin signaling observed in mouse mod-
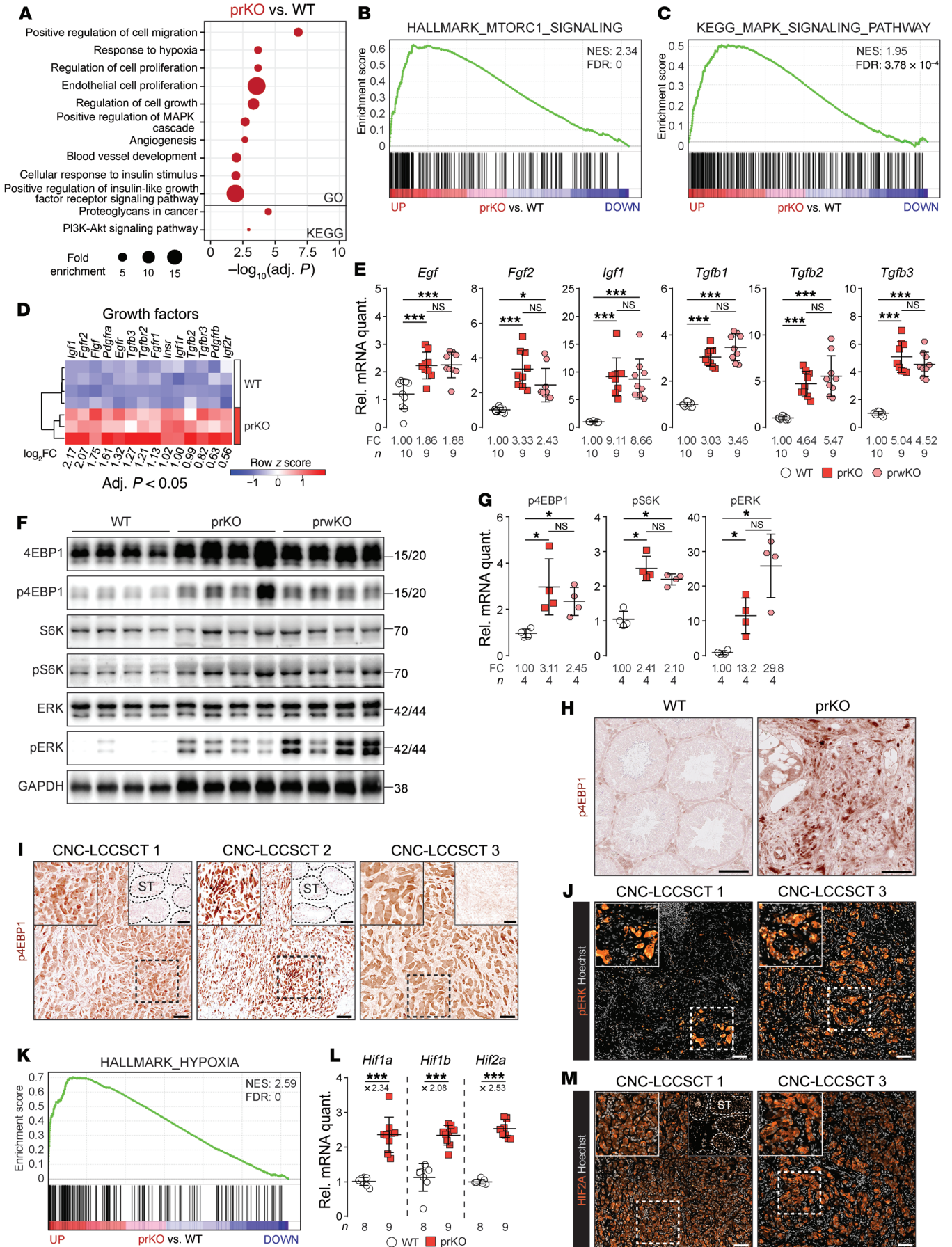
Figure 8. PKA activation induces mTOR, MAPK, and hypoxia pathways in tumor of human LCCSCTs. (**A**) GO enrichment scores of tumor development–associated pathways based on gene list specifically deregulated in 2-month-old prKO testis compared with srKO and lrKO testes. (**B** and **C**) GSEA of microarray gene expression data showing positive enrichment of hallmark-MTORC1 signaling gene list (**B**) and KEGG-MAPK signaling pathway gene list (**C**) in 2-month-old prKO testis compared with WT. (**D**) Heatmap representing the median-centered expression of significantly deregulated growth factors and associated receptors (adj. $P < 0.05$) in 2-month-old prKO ($n = 3$–4) compared with WT ($n = 4$). (**E**) RT-qPCR analysis of *Egf*, *Fgf2*, *Igf1*, *Tgfb1*, *Tgfb2*, and *Tgfb3* transcripts in 4-month-old WT, prKO, and prwKO testes. One-way ANOVA was followed by Tukey's multiple-correction test, Welch's 1-way ANOVA was followed by Games-Howell multiple-correction test, and Kruskal-Wallis test was followed by Dunn's multiple-correction test. (**F**) Western blot analysis of p4EBP1, pS6K, and pERK accumulation in 4-month-old WT, prKO, and prwKO testes. (**G**) Phosphorylated protein quantification over total proteins. Statistical analysis was performed using Student's *t* test. (**H**) Immunohistochemical detection of p4EBP1 in 4-month-old WT and prKO testes. (**I** and **J**) Immunohistochemical detection of p4EBP1 and pERK in CNC-LCCSCTs. Insets at the top right (**I**) correspond to areas adjacent to the tumor characterized by low p4EBP1 staining. (**K**) GSEA of microarray gene expression data showing positive enrichment of hallmark-hypoxia gene list (genes upregulated in response to hypoxia) in 2-month-old prKO testis compared with WT. (**L**) *Hif1a*, *Hif1b*, and *Hif2a* transcript analysis in 4-month-old WT and prKO testes. Statistical analysis was performed using Welch's or Student's *t* test. (**M**) Immunohistochemical detection of HIF2A in CNC-LCCSCTs. Bars represent the mean per group ± SD. Scale bars: 100 μm. Original magnification, ×1.60 (left insets, **I**, **J**, and **M**); ×0.80 (right insets, **I** and **M**). *$P < 0.05$; ***$P < 0.001$.

els developed by Tanwar and colleagues and Boyer and colleagues (42, 74). In particular, the *Prkar1a* mutant SCs display an early and much higher increase of *Inha* transcripts than any other TGF-β family genes. This could play a major role in limiting SC proliferation induced by the WNT/β-catenin pathway, as suggested by previous studies on inhibin-α autocrine actions (75, 76). In addition, previously defined molecular signatures attesting to SC maturation under the control of androgens (73, 77, 78) and thyroid hormone (79, 80) remain unchanged in srKO and prKO transcriptomes at the prepubertal stage (2 weeks), but increase at adulthood. Finally, whether PKA-induced *Wnt4* expression results from PKA-dependent increased *Ctnnb1* expression and/or PKA-mediated β-catenin activation mechanisms, as described in ovarian granulosa and luteal cells (81–83), remains to be explored for *Prkar1a*⁻/⁻ SCs. In contrast to the srKO and lrKO models, prKO mice develop testicular tumors with histological and molecular characteristics similar to those of LCCSCTs of CNC patients. This indicates that tumor onset is dependent on both SC and stromal proliferative signals activated by *Prkar1a* loss in both testicular compartments. This unprecedented situation in genetic models of testicular tumors underlines the role of paracrine interactions in CNC-LCCSCT pathogenesis. Among the upregulated signals in response to *Prkar1a* loss, *Wnt4* expression is present at significantly higher levels in the prKO than in the srKO model and increases in parallel with tumor development, suggesting that tumor cells could be an additional source of the WNT4 signal. Indeed, our IHC analyses on human CNC-LCCSCT biopsies confirm that WNT4 is accumulated in cells within the tumor mass. This increase in the WNT4 signal is associated with an increase in the expression of WNT/β-catenin responsive genes and therefore

raises the question of its involvement in tumor promotion of LCCSCTs. The double-mutant prwKO model study demonstrates that the WNT4 signal is a limiting component in the growth factor set that conditions CNC-LCCSCT development. Indeed, in the prwKO testis, *Wnt4* loss abolishes tumor formation and drastically reduces the stromal proliferation rate compared with in the prKO testis. Importantly, *Wnt4* loss does not prevent the overall WNT/β-catenin pathway activation in the prwKO testis, given that the WNT5A ligand remains produced in excess and that PKA-dependent phosphorylation can directly favor β-catenin stabilization (84). In this context, it can be assumed that *Wnt4* inactivation sufficiently reduces the strength of the pathway to slow down stromal proliferation below a limiting threshold for tumor formation. Residual stromal hyperplasia in the double-mutant testis also confirms the impact of additional PKA-activated growth signals independently of *Wnt4* expression. Previously, a mouse model (*Ctnnb1*^tm1Mmt/+; *Tg[AMH-cre]1Flor*) expressing a stabilized form of β-catenin targeted in SCs developed testicular cancers with molecular and invasive characteristics different from those found in tumors of the prKO model and human CNC-LCCSCT and that arose independently of the influence of the stromal compartment (85). In humans, while *WNT4* duplications have been associated with chromosome 46, XY testicular dysgenesis and ambiguous external genitalia occur beginning with fetal development, and despite the recurrent *CTNNB1*-activating mutations in SCST cells (86), WNT4-activating mutations remain poorly documented in testicular cancer, unlike in other tissues, i.e., ovaries (87). These observations reinforce the idea that, although the WNT4 signal is a mandatory actor, it does not support on its own the formation of the LCCSCT.

Although *Fgf2*, *Egf*, *Igf1*, and *Tgfb1-3* gene expression was also strongly upregulated in prKO testes, it remained elevated in prwKO testes, suggesting that it could participate in maintaining the moderate proliferation observed in the prwKO residual stromal hyperplasia. A functional cooperation of WNT4 and TGF-β pathways in tumor growth and in its fibrotic enrichment is not excluded. Indeed, studies showed that the TGF-β/SMAD3 pathway mobilized the WNT/β-catenin pathway in smooth muscle cell proliferation (88) and in the development of pathological dermal fibrosis in a p38-dependent manner by decreasing the accumulation of WNT pathway negative regulators (89). In the prwKO testis, tumor suppression is associated with a systematic reduction in the fibrotic areas that characterizes LCCSCTs. Consistent with the increase of FGF2, EGF, IGF1, and KIT-L, their converging signaling pathways (MAPK and PI3K/AKT/mTOR; ref. 90) are activated in the LCCSCTs of CNC patients and prKO mice, supporting their involvement in tumoral expansion. In addition, several studies in different tissues have shown that TGF-β signaling activates the expression of *miR-21* targeting PTEN production and activity, lifting the inhibition of AKT/mTORC1 signaling, which in turn amplifies the oncogenic signal, matrix protein synthesis, and fibrosis (91, 92). As revealed by the prKO transcriptomic analyses, *miR-21* upregulation argues in favor of such a TGF-β/mTOR crosstalk in the development of CNC-LCCSCTs (NCBI's Gene Expression Omnibus [GEO] GSE159150). The mTOR pathway was previously shown to be activated in SCs in response to *Lkb1* inactivation in a study aiming to understand the molecular mechanisms involved in testicular alterations in PJS (52). In this study, mTOR pathway activation induced by disruption

of the LKB1/AMPK pathway resulted in SC polarity and BTB alterations, resumption of their proliferative activities, and loss of germ cells. However, no LCCSCT-type tumorigenesis was shown in this work, suggesting that, as in CNC-LCCSCTs, PJS-LCCSCT development could be dependent on signals activated by the mutation that should be present both in SCs and other testicular compartments. In the prKO model, PKA-induced mTORC1 pathway activation in both the tumor and in SCs does not imply any alteration of the expression nor activity of AMPK, indicating that *Prkar1a* and *Lkb1* mutations lead to mTOR pathway mobilization by a different way. In previous work examining the molecular consequences of *Prkar1a* loss in the adrenal cortex leading to primary pigmented nodular adrenocortical disease (PPNAD) lesions, we showed that PKA activity triggers an increase in TGF-β family member expression and directly activates mTORC1 to promote cell survival (93, 94). Intriguingly and in contrast with our present results in testis, we previously showed a marked reciprocal antagonism of the WNT/β-catenin and PKA pathways in adrenocortical zonation and tumorigenesis (95), since *Prkar1a* inactivation in the adrenal cortex represses zona glomerulosa identity and opposes the prooncogenic action of WNT/β-catenin signaling. Our work suggests that in the CNC, the molecular modalities of PKA action in PPNAD and LCCSCT expansion do not fully overlap. This incomplete overlap would probably rely on nonidentical PKA-controlled key networks involved in tissue homeostasis of adrenal and testis that yet arise from common primordium. In this context, the question of WNT-PKA cooperation in the pathogenesis of the CNC ovary remains unanswered.

In conclusion, our data demonstrate that the chronic unrepressed PKA activity in somatic testis cells of CNC patients unbalances testicular homeostasis by generating a gonadal paracrine network crisis that includes an aberrant postnatal WNT4 signal acting as a driving force for shaping intratubular lesions and tumor expansion.

Methods

Mice. Sf1:Cre (95), *Amh:Cre* (22), or *Scc:Cre* (23), *Prkar1a^{fl/fl}* (9), *Wnt4^{fl/fl}* (96), and *Prkaca^{+/-}* mice (97) have been described previously. The following mouse crossings were enabled to generate multiple models: prKO (*Sf1:Cre,Prkar1a^{fl/fl}*, progenitor cell <u>R1a</u> <u>KO</u>), prKO/*Prkaca^{+/-}* (*Sf1:Cre,Prkar1a^{fl/fl},Prkaca^{+/-}* with global *Prkaca* haploinsufficiency), srKO (*Amh:Cre,Prkar1a^{fl/fl}*, SC <u>R1a KO</u>), lrKO (*Scc:Cre,Prkar1a^{fl/fl}*, <u>LC R1a KO</u>), double-mutant prwKO (*Sf1:Cre,Prkar1a^{fl/fl},Wnt4^{fl/fl}*), and srwKO (*Amh:Cre,Prkar1a^{fl/fl},Wnt4^{fl/fl}*). Mouse models used are listed in Supplemental Table 1. Mouse models were enriched with the *Rosa26R-mtmg* system to follow recombination events. Control animals were *Prkar1a^{fl/fl}* or *Prkar1a^{fl/fl},Wnt4^{fl/fl}* littermates, depending on experiments.

Samples from patients. Histological slides of testis lesions were obtained from 3 CNC patients. Human adult healthy testis sections were used as controls for histological analyses (UM-HuFPT151, CliniSciences). The clinical data summary of CNC patients is provided in Supplemental Table 2.

Hormonal measurements. Mice were euthanized by decapitation, and blood was collected between 9:00 am and 10:00 am, since animals were maintained on a 12-hour light (07:00 am to 7:00 pm)/12-hour dark cycle. Plasma testosterone concentrations were determined using an ELISA kit. Plasma LH and FSH concentrations were determined using a multiplex assay (MPTMAG-49K, Merck Millipore).

Histology. Testes were embedded in paraffin, and 5 μm sections were prepared. H&E, Masson's trichrome, alizarin red S, and toluidine blue stainings were performed depending on experiments. Detailed descriptions of immunohistochemistry and TUNEL staining are provided in the Supplemental Methods and Supplemental Table 3.

Microarray analyses. Gene expression profiles for 2-week-old and 2-month-old WT, prKO, srKO, and lrKO testes were analyzed using Affymetrix Mouse Gene 2.0 ST arrays. Raw and processed data have been deposited in NCBI's GEO database (GSE159150). Further description of methods is provided in Supplemental Methods.

RT-qPCR. Total mRNAs were extracted and reverse transcribed as previously described (95). Primers used are listed in Supplemental Table 4. Relative gene expression was obtained by the ΔΔCt method with normalization to average expression of actin.

Western blot. Thirty micrograms of total proteins were loaded on 8% SDS-PAGE gel, transferred on nitrocellulose, and detected with primary antibodies (Supplemental Table 3). Signals were quantified with the ChemiDoc MP Imaging System camera system and Image Lab software (Bio-Rad).

Statistics. Statistical analyses were performed using R and GraphPad Prism 8. Numbers of mice per group are reported in the figures. All bars represent the mean ± SD. Normality of data was assessed using the Shapiro-Wilk normality test. For comparison of 2 groups, variance equality was tested using the *F* test. Statistical analysis of 2 groups was performed by 2-tailed Student's *t* test with or without Welch's correction (as a function of variance) for normally distributed data or by Mann-Whitney *U* test for not normally distributed data. For comparison of multiple groups, variance equality was tested using the Brown-Forsythe test. Statistical analysis of multiple groups was performed by 1-way ANOVA followed by Tukey's multiple-correction test or Welch's 1-way ANOVA followed by the Games-Howell multiple-correction test (as a function of variance) for normally distributed data or by Kruskal-Wallis test followed by Dunn's multiple-correction test for not normally distributed data. Statistical analysis of hyperplasia/tumor proportion was performed by 2-proportion Fisher's test.

Study approval. All patients underwent tumor resection and gave informed consent for the use of their resected tissues for research purposes. Mouse experiments were conducted according to French and European directives for the use and care of animals for research purposes and were approved by the Comité d'Éthique pour l'Expérimentation Animale en Auvergne, C2EA-02, at Institut National de Recherche pour l'Agriculture, l'Alimentation et l'Environnement, Research Center Clermont-Theix, France (C2E2A).

Address correspondence to: Anne-Marie Lefrançois-Martinez, GReD Institute, 28 place Henri Dunant, Faculté de Médecine-CRBC 63001 Clermont Ferrand CEDEX 01, France. Phone: 33.0.4.73.40.77.59; Email: a-marie.lefrancois-martinez@uca.fr.

1. Bertherat J, et al. Mutations in regulatory subunit type 1A of cyclic adenosine 5′-monophosphate-dependent protein kinase (PRKAR1A): phenotype analysis in 353 patients and 80 different genotypes. *J Clin Endocrinol Metab*. 2009;94(6):2085–2091.

2. Stratakis CA, et al. Clinical and molecular features of the Carney complex: diagnostic criteria and recommendations for patient evaluation. *J Clin Endocrinol Metab*. 2001;86(9):4041–4046.

3. Boikos SA, Stratakis CA. Carney complex: the first 20 years. *Curr Opin Oncol*. 2007;19(1):24–29.

4. Correa R, et al. Carney complex: an update. *Eur J Endocrinol*. 2015;173(4):M85–M97.

5. Ulbright TM, et al. Intratubular large cell hyalinizing Sertoli cell neoplasia of the testis: a report of 8 cases of a distinctive lesion of the Peutz-Jeghers syndrome. *Am J Surg Pathol*. 2007;31(6):827–835.

6. Gourgari E, et al. Large-cell calcifying Sertoli cell tumors of the testes in pediatrics. *Curr Opin Pediatr*. 2012;24(4):518–522.

7. Carney JA, et al. The complex of myxomas, spotty pigmentation, and endocrine overactivity. *Medicine (Baltimore)*. 1985;64(4):270–283.

8. Kratzer SS, et al. Large cell calcifying Sertoli cell tumor of the testis: contrasting features of six malignant and six benign tumors and a review of the literature. *Am J Surg Pathol*. 1997;21(11):1271–1280.

9. Kirschner LS, et al. A mouse model for the Carney complex tumor syndrome develops neoplasia in cyclic AMP-responsive tissues. *Cancer Res*. 2005;65(11):4506–4514.

10. Amieux PS, McKnight GS. The essential role of RI alpha in the maintenance of regulated PKA activity. *Ann N Y Acad Sci*. 2002;968:75–95.

11. Mesa H, et al. Comparative immunomorphology of testicular Sertoli and sertoliform tumors. *Hum Pathol*. 2017;61:181–189.

12. Idrees MT, et al. The World Health Organization 2016 classification of testicular non-germ cell tumours: a review and update from the International Society of Urological Pathology Testis Consultation Panel. *Histopathology*. 2017;70(4):513–521.

13. Roth LM, et al. Perspectives on testicular sex cord-stromal tumors and those composed of both germ cells and sex cord-stromal derivatives with a comparison to corresponding ovarian neoplasms. *Hum Pathol*. 2017;65:1–14.

14. Toppari J, et al. Inhibin gene expression in a large cell calcifying Sertoli cell tumour and serum inhibin and activin levels. *APMIS*. 1998;106(1):101–112.

15. Sato K, et al. Large cell calcifying Sertoli cell tumor of the testis: comparative immunohistochemical study with Leydig cell tumor. *Pathol Int*. 2005;55(6):366–371.

16. Rotgers E, et al. At the crossroads of fate-somatic cell lineage specification in the fetal gonad. *Endocr Rev*. 2018;39(5):739–759.

17. Nordhoff V, et al. Constitutively active mutations of G protein-coupled receptors: the case of the human luteinizing hormone and follicle-stimulating hormone receptors. *Arch Med Res*. 1999;30(6):501–509.

18. Huhtaniemi I, et al. Genetically modified mouse models in studies of luteinising hormone action. *Mol Cell Endocrinol*. 2006;252(1–2):126–135.

19. Casarini L, et al. Effects of polymorphisms in gonadotropin and gonadotropin receptor genes on reproductive function. *Rev Endocr Metab Disord*. 2011;12(4):303–321.

20. McGee SR, Narayan P. Precocious puberty and Leydig cell hyperplasia in male mice with a gain of function mutation in the LH receptor gene. *Endocrinology*. 2013;154(10):3900–3913.

21. Bingham NC, et al. Development of a steroidogenic factor 1/Cre transgenic mouse line. *Genesis*. 2006;44(9):419–424.

22. Lécureuil C, et al. Sertoli and granulosa cell-specific Cre recombinase activity in transgenic mice. *Genesis*. 2002;33(3):114–118.

23. Buaas FW, et al. In vivo evidence for the crucial role of SF1 in steroid-producing cells of the testis, ovary and adrenal gland. *Development*. 2012;139(24):4561–4570.

24. Mruk DD, Cheng CY. The mammalian blood-testis barrier: its biology and regulation. *Endocr Rev*. 2015;36(5):564–591.

25. Cai J,et al. Increased expression of dermatopontin and its implications for testicular dysfunction in mice. *Mol Med Rep*. 2016;13(3):2431–2438.

26. Takeuchi T, et al. Extracellular matrix dermatopontin modulates prostate cell growth in vivo. *J Endocrinol*. 2006;190(2):351–361.

27. Zhou W, et al. Changes in gene expression in somatic cells of rat testes resulting from hormonal modulation and radiation-induced germ cell depletion. *Biol Reprod*. 2010;82(1):54–65.

28. Ohta H, et al. Regulation of proliferation and differentiation in spermatogonial stem cells: the role of c-kit and its ligand SCF. *Development*. 2000;127(10):2125–2131.

29. Dolci S, et al. Signaling through extracellular signal-regulated kinase is required for spermatogonial proliferative response to stem cell factor. *J Biol Chem*. 2001;276(43):40225–40233.

30. Sato T, et al. Testis tissue explantation cures spermatogenic failure in c-Kit ligand mutant mice. *Proc Natl Acad Sci U S A*. 2012;109(42):16934–16938.

31. Cardoso HJ, et al. The stem cell factor (SCF)/c-KIT signalling in testis and prostate cancer. *J Cell Commun Signal*. 2017;11(4):297–307.

32. Morales JK, et al. Mast cell homeostasis and the JAK-STAT pathway. *Genes Immun*. 2010;11(8):599–608.

33. Yan W, et al. Stage-specific regulation of stem cell factor gene expression in the rat seminiferous epithelium. *Endocrinology*. 1999;140(3):1499–1504.

34. Grimaldi P, et al. Cyclic adenosine monophosphate (cAMP) stimulation of the kit ligand promoter in sertoli cells requires an Sp1-binding region, a canonical TATA box, and a cAMP-induced factor binding to an immediately downstream GC-rich element. *Biol Reprod*. 2003;69(6):1979–1988.

35. Walczak EM, et al. Wnt signaling inhibits adrenal steroidogenesis by cell-autonomous and non-cell-autonomous mechanisms. *Mol Endocrinol*. 2014;28(9):1471–1486.

36. Mizusaki H, et al. Dax-1 (dosage-sensitive sex reversal-adrenal hypoplasia congenita critical region on the X chromosome, gene 1) gene transcription is regulated by wnt4 in the female developing gonad. *Mol Endocrinol*. 2003;17(4):507–519.

37. Gallegos TF, et al. A protein kinase A and Wnt-dependent network regulating an intermediate stage in epithelial tubulogenesis during kidney development. *Dev Biol*. 2012;364(1):11–21.

38. Yu HF, et al. Bmp2 regulates Serpinb6b expression via cAMP/PKA/Wnt4 pathway during uterine decidualization. *J Cell Mol Med*. 2020;24(12):7023–7033.

39. Rajaram RD, et al. Progesterone and Wnt4 control mammary stem cells via myoepithelial crosstalk. *EMBO J*. 2015;34(5):641–652.

40. Vainio S, et al. Female development in mammals is regulated by Wnt-4 signalling. *Nature*. 1999;397(6718):405–409.

41. Liu CF, et al. Sex-specific roles of beta-catenin in mouse gonadal development. *Hum Mol Genet*. 2009;18(3):405–417.

42. Boyer A, et al. CTNNB1 signaling in sertoli cells downregulates spermatogonial stem cell activity via WNT4. *PLoS One*. 2012;7(1):e29764.

43. Kimura T, et al. The stabilization of beta-catenin leads to impaired primordial germ cell development via aberrant cell cycle progression. *Dev Biol*. 2006;300(2):545–553.

44. Chassot AA, et al. Constitutive WNT/CTNNB1 activation triggers spermatogonial stem cell proliferation and germ cell depletion. *Dev Biol*. 2017;426(1):17–27.

45. Corda G, Sala A. Non-canonical WNT/PCP signalling in cancer: Fzd6 takes centre stage. *Oncogenesis*. 2017;6(7):e364.

46. Pitetti JL, et al. An essential role for insulin and IGF1 receptors in regulating sertoli cell proliferation, testis size, and FSH action in mice. *Mol Endocrinol*. 2013;27(5):814–827.

47. Khan SA, et al. Follicle-stimulating hormone amplifies insulin-like growth factor I–mediated activation of AKT/protein kinase B signaling in immature rat Sertoli cells. *Endocrinology*. 2002;143(6):2259–2267.

48. Wandzioch E, et al. Activation of the MAP kinase pathway by c-Kit is PI-3 kinase dependent in hematopoietic progenitor/stem cell lines. *Blood*. 2004;104(1):51–57.

49. Cannarella R, et al. Effects of the insulin-like growth factor system on testicular differentiation and function: a review of the literature. *Andrology*. 2018;6(1):3–9.

50. Boyer A, et al. mTOR regulates gap junction alpha-1 protein trafficking in sertoli cells and is required for the maintenance of spermatogenesis in mice. *Biol Reprod*. 2016;95(1):13.

51. Mok KW, et al. Regulation of blood-testis barrier (BTB) dynamics during spermatogenesis via the "Yin" and "Yang" effects of mammalian target of rapamycin complex 1 (mTORC1) and mTORC2. *Int Rev Cell Mol Biol*. 2013;301:291–358.

52. Tanwar PS, et al. Altered LKB1/AMPK/TSC1/TSC2/mTOR signaling causes disruption of Sertoli cell polarity and spermatogenesis. *Hum Mol Genet*. 2012;21(20):4394–4405.

53. Washecka R, et al. Testicular tumors in Carney's complex. *J Urol*. 2002;167(3):1299–1302.

54. Griffin KJ, et al. Down-regulation of regulatory subunit type 1A of protein kinase A leads to endocrine and other tumors. *Cancer Res*. 2004;64(24):8811–8815.

55. Burton KA, et al. Haploinsufficiency at the protein kinase A RI alpha gene locus leads to fertility defects in male mice and men. *Mol Endocrinol*. 2006;20(10):2504–2513.

56. Wieacker P, et al. Male infertility as a component of Carney complex. *Andrologia*. 2007;39(5):196–197.

57. Kumar TR, et al. Transgenic models to study gonadotropin function: the role of follicle-stimulating hormone in gonadal growth and tumorigenesis. *Mol Endocrinol*. 1999;13(6):851–865.

58. Haywood M, et al. An activated human follicle-stimulating hormone (FSH) receptor stimulates FSH-like activity in gonadotropin-deficient transgenic mice. *Mol Endocrinol*. 2002;16(11):2582–2591.

59. Huhtaniemi IT, Aittomäki K. Mutations of follicle-stimulating hormone and its receptor: effects on gonadal function. *Eur J Endocrinol*. 1998;138(5):473–481.

60. Siegel ET, et al. The molecular basis of impaired follicle-stimulating hormone action: evidence from human mutations and mouse models. *Reprod Sci*. 2013;20(3):211–233.

61. Gromoll J, et al. An activating mutation of the follicle-stimulating hormone receptor autonomously sustains spermatogenesis in a hypophysectomized man. *J Clin Endocrinol Metab*. 1996;81(4):1367–1370.

62. Oduwole OO, et al. Role of follicle-stimulating hormone in spermatogenesis. *Front Endocrinol*. 2018;9:763.

63. Mullaney BP, Skinner MK. Basic fibroblast growth factor (bFGF) gene expression and protein production during pubertal development of the seminiferous tubule: follicle-stimulating hormone-induced Sertoli cell bFGF expression. *Endocrinology*. 1992;131(6):2928–2934.

64. Rossi P, et al. Follicle-stimulating hormone induction of steel factor (SLF) mRNA in mouse Sertoli cells and stimulation of DNA synthesis in spermatogonia by soluble SLF. *Dev Biol*. 1993;155(1):68–74.

65. Tadokoro Y, et al. Homeostatic regulation of germinal stem cell proliferation by the GDNF/FSH pathway. *Mech Dev*. 2002;113(1):29–39.

66. Plotton I, et al. Decrease of both stem cell factor and clusterin mRNA levels in testicular biopsies of azoospermic patients with constitutive or idiopathic but not acquired spermatogenic failure. *Hum Reprod*. 2006;21(9):2340–2345.

67. Bhattacharya I, et al. A switch in Sertoli cell responsiveness to FSH may be responsible for robust onset of germ cell differentiation during prepubartal testicular maturation in rats. *Am J Physiol Endocrinol Metab*. 2012;303(7):E886–E898.

68. Jorgez CJ, et al. E2F1 regulates testicular descent and controls spermatogenesis by influencing WNT4 signaling. *Development*. 2021;148(1):dev191189.

69. Li Y, et al. The sex-determining factors SRY and SOX9 regulate similar target genes and promote testis cord formation during testicular differentiation. *Cell Rep*. 2014;8(3):723–733.

70. Barrionuevo F, et al. Homozygous inactivation of Sox9 causes complete XY sex reversal in mice. *Biol Reprod*. 2006;74(1):195–201.

71. Moniot B, et al. The PGD2 pathway, independently of FGF9, amplifies SOX9 activity in Sertoli cells during male sexual differentiation. *Development*. 2009;136(11):1813–1821.

72. Gonen N, et al. Sex reversal following deletion of a single distal enhancer of *Sox9*. *Science*. 2018;360(6396):1469–1473.

73. Willems A, et al. Selective ablation of the androgen receptor in mouse sertoli cells affects sertoli cell maturation, barrier formation and cytoskeletal development. *PLoS One*. 2010;5(11):e14168.

74. Tanwar PS, et al. Constitutive WNT/beta-catenin signaling in murine Sertoli cells disrupts their differentiation and ability to support spermatogenesis. *Biol Reprod*. 2010;82(2):422–432.

75. Cai K, et al. Action mechanism of inhibin α-subunit on the development of Sertoli cells and first wave of spermatogenesis in mice. *PLoS One*. 2011;6(10):e25585.

76. Namwanje M, Brown CW. Activins and inhibins: roles in development, physiology, and disease. *Cold Spring Harb Perspect Biol*. 2016;8(7):a021881.

77. Vija L, et al. Ligand-dependent stabilization of androgen receptor in a novel mouse ST38c Sertoli cell line. *Mol Cell Endocrinol*. 2014;384(1–2):32–42.

78. Edelsztein NY, Rey RA. Importance of the androgen receptor signaling in gene transactivation and transrepression for pubertal maturation of the testis. *Cells*. 2019;8(8):861.

79. Meroni SB, et al. Molecular mechanisms and signaling pathways involved in sertoli cell proliferation. *Front Endocrinol (Lausanne)*. 2019;10:224.

80. Hernandez A, Martinez ME. Thyroid hormone action in the developing testis: intergenerational epigenetics. *J Endocrinol*. 2020;244(3):R33–R46.

81. Parakh TN, et al. Follicle-stimulating hormone/cAMP regulation of aromatase gene expression requires beta-catenin. *Proc Natl Acad Sci U S A*. 2006;103(33):12435–12440.

82. Roy L, et al. Convergence of 3′,5′-cyclic adenosine 5′-monophosphate/protein kinase A and glycogen synthase kinase-3beta/beta-catenin signaling in corpus luteum progesterone synthesis. *Endocrinology*. 2009;150(11):5036–5045.

83. Boyer A, et al. WNT4 is required for normal ovarian follicle development and female fertility. *FASEB J*. 2010;24(8):3010–3025.

84. Hino S, et al. Phosphorylation of beta-catenin by cyclic AMP-dependent protein kinase stabilizes beta-catenin through inhibition of its ubiquitination. *Mol Cell Biol*. 2005;25(20):9063–9072.

85. Chang H, et al. Overactive beta-catenin signaling causes testicular sertoli cell tumor development in the mouse. *Biol Reprod*. 2009;81(5):842–849.

86. Perrone F, et al. Frequent mutation and nuclear localization of β-catenin in sertoli cell tumors of the testis. *Am J Surg Pathol*. 2014;38(1):66–71.

87. McMellen A, et al. Wnt signaling in gynecologic malignancies. *Int J Mol Sci*. 2020;21(12):4272.

88. DiRenzo DM, et al. A crosstalk between TGF-β/Smad3 and Wnt/β-catenin pathways promotes vascular smooth muscle cell proliferation. *Cell Signal*. 2016;28(5):498–505.

89. Akhmetshina A, et al. Activation of canonical Wnt signalling is required for TGF-β–mediated fibrosis. *Nat Commun*. 2012;3:735.

90. Witsch E, et al. Roles for growth factors in cancer progression. *Physiology (Bethesda)*. 2010;25(2):85–101.

91. Woodcock HV, et al. The mTORC1/4E-BP1 axis represents a critical signaling node during fibrogenesis. *Nat Commun*. 2019;10(1):6.

92. Dey N, et al. microRNA-21 governs TORC1 activation in renal cancer cell proliferation and invasion. *PLoS One*. 2012;7(6):e37366.

93. Sahut-Barnola I, et al. Cushing's syndrome and fetal features resurgence in adrenal cortex-specific Prkar1a knockout mice. *PLoS Genet*. 2010;6(6):e1000980.

94. de Joussineau C, et al. mTOR pathway is activated by PKA in adrenocortical cells and participates in vivo to apoptosis resistance in primary pigmented nodular adrenocortical disease (PPNAD). *Hum Mol Genet*. 2014;23(20):5418–5428.

95. Drelon C, et al. PKA inhibits WNT signalling in adrenal cortex zonation and prevents malignant tumour development. *Nat Commun*. 2016;7(1):1–14.

96. Shan J, et al. Generation of an allele to inactivate Wnt4 gene function conditionally in the mouse. *Genesis*. 2009;47(11):782–788.

97. Skålhegg BS, et al. Mutation of the Calpha subunit of PKA leads to growth retardation and sperm dysfunction. *Mol Endocrinol*. 2002;16(3):630–639.